CAPITAL UNIVERSITY OF SCIENCE AND TECHNOLOGY, ISLAMABAD

Eudragit L-100 Nanoparticles for Improved Bioavailability and Pharmacokinetics of Loperamide

by

Asadullah

A thesis submitted in partial fulfillment for the degree of Master of Philosophy

in the

Faculty of Pharmacy

Department of Pharmacy

2025

CERTIFICATE OF APPROVAL

Eudragit L-100 Nanoparticles for Improved Bioavailability and Pharmacokinetics of Loperamide

by

Asadullah

(Registration No: MPH233018)

THESIS EXAMINING COMMITTEE

S. No.	Examiner	Name	Organization
(a)	External Examiner	Dr. Muhammad Iqbal Nasiri	HU, Islamabad
(b)	Internal Examiner	Dr. Muhammad Saalim	CUST, Islamabad
(c)	Supervisor	Dr. Mahira Zeeshan	CUST, Islamabad

Dr. Mahira Zeeshan
Thesis Supervisor
October, 2025

Dr. Nadia Shamshad Malik
Head
Dept. of Pharmaceutics
October, 2025

Dr. Muzaffar Abbas
Dean
Faculty of Pharmacy
October, 2025

Author's Declaration

I, **Asadullah** hereby state that my MPhil thesis titled "**Eudragit L-100 Nanoparticles for Improved Bioavailability and Pharmacokinetics of Loperamide**" is my own work and has not been submitted previously by me for taking any degree from Capital University of Science and Technology, Islamabad or anywhere else in the country/abroad.

At any time if my statement is found to be incorrect even after my graduation, the University has the right to withdraw my MPhil Degree.

(Asadullah)

Registration No: MPH233018

Plagiarism Undertaking

I solemnly declare that research work presented in this thesis titled "**Eudragit L-100 Nanoparticles for Improved Bioavailability and Pharmacokinetics of Loperamide**" is solely my research work with no significant contribution from any other person. Small contribution/help wherever taken has been duly acknowledged and that complete thesis has been written by me.

I understand the zero tolerance policy of the HEC and Capital University of Science and Technology towards plagiarism. Therefore, I as an author of the above titled thesis declare that no portion of my thesis has been plagiarized and any material used as reference is properly referred/cited.

I undertake that if I am found guilty of any formal plagiarism in the above titled thesis even after award of MPhil Degree, the University reserves the right to withdraw/revoke my MPhil degree and that HEC and the University have the right to publish my name on the HEC/University website on which names of students are placed who submitted plagiarized work.

(Asadullah)

Registration No: MPH233018

Acknowledgement

In the name of **Allah**, the Most Gracious, the Most Merciful. All praises and thanks to Almighty Allah, who granted me the strength, patience, and wisdom to complete this thesis. My deepest respect and gratitude go to the **Holy Prophet Muhammad** whose teachings inspire us to seek knowledge and serve humanity.

I am profoundly grateful to my parents, whose endless prayers, love, sacrifices, and unwavering support have been the foundation of my achievements. Without their encouragement, this journey would not have been possible.

My heartfelt thanks to my supervisor, **Dr. Mahira Zeeshan**, Assistant Professor, Faculty of Pharmaceutical Sciences, Capital University of Science and Technology, Islamabad, for her valuable guidance, encouragement, and insightful feedback throughout this research. Her mentorship has been instrumental in shaping this work.

I also extend my appreciation to all my teachers and academic staff, whose dedication to teaching and sharing knowledge has greatly enriched my learning experience.

I am thankful to the QC Lab at Davis Pharmaceutical Laboratories, Islamabad, for providing necessary resources and technical support that made this research possible.

Special thanks to my friends and colleagues for their moral support, cooperation, and for making this journey enjoyable and memorable. Lastly, I express my gratitude to everyone who directly or indirectly contributed to the completion of this thesis. May Allah bless you all abundantly.

(Asadullah)

Abstract

This research addresses the challenges to orally deliver the drug, Loperamide (LPM), due to its poor water solubility and significant first-pass metabolism, which severely limits its effectiveness as an antidiarrheal. To overcome LPM bioavailability problem, a nano-formulation, LPM-loaded Eudragit® L-100 (LPM-L-E NPs), was developed using Eudragit® L-100 by a solvent evaporation method. Eudragit® L-100 was chosen for its ability to dissolve at pH levels above 6, ensuring the drug is protected in the acidic stomach and released specifically in the intestines. The developed nanoparticles were approximately 312 nm in size with good stability. They demonstrated an impressive entrapment efficiency of about 99.56%. Analysis confirmed successful encapsulation, and the LPM was transformed into an amorphous state inside the nanoparticles, which facilitated in diffusion and dissolution of the drug across the nanoparticles. The nanoparticles were also observed to be spherical and smooth. In vitro studies showed minimal LPM release in stomach-like conditions (pH 1.2), preventing premature degradation. However, at intestinal pH (6.8), a sustained drug release over 48 hours was observed, confirming the pH-responsive nature of the formulation. In vivo pharmacokinetic evaluations in rats further highlighted the benefits. Compared to a standard LPM suspension, the LPM-L-E NPs achieved significantly higher drug levels in the bloodstream (C max of 26.06 μg/ml vs. 3.36 μg/ml), a longer half-life (11.7 hours vs. 6.5 hours), and dramatically increased overall drug exposure (AUC 568.46 vs. 22.68 μg·h/ml). These results indicate superior bioavailability, suggesting the possibility of less frequent dosing, which could improve patient adherence and reduce side effects. In conclusion, this study successfully created and optimized pH-sensitive Eudragit L-100 nanoparticles for LPM. This innovative approach significantly improves LPM's solubility, protects it from gastric degradation, and substantially enhances its systemic bioavailability. This breakthrough provides a promising foundation for using pH-sensitive nanoparticle systems to improve the oral delivery of other poorly water-soluble drugs, warranting further investigation.

Contents

List of Figures

List of Tables

Abbreviations

API	Active pharmaceutical Ingredients
BCS	Biopharmaceutics Classification System
LPM	Loperamide
LPM-L-E-NPS	Loperamide-loaded Eudragit L-100 Nanoparticles
NCA	Non-Compartmental Analysis
NLC's	Nano Lipid Carriers
PBCA	Polybutylcyanoacrylate
PCL	Polycaprolactone
PDI	Polydispersity Index
PLGA	Polylactide-coglycolide
PVA	Polyvinyl Alcohol
SFAES	Sorbitan Fatty Acid Esters
SLNS	Solid Lipid Carriers
XPRD	X-ray Powder Diffractometer

Symbols

$\mathbf{AUC}_{0-t}$	Area Under the Curve From Time Zero to the Last Quantifiable Concentration
$\mathbf{AUC}_{0-\infty}$	Area Under the Curve From Time Zero to Infinity
$\mathbf{AUMC}_{0-\infty}$	Area Under the First Moment Curve From Time Zero to Infinity
$\mathbf{Cl/F}$	Apparent Clearance
$\mathbf{C}_{\max}$	Maximum Concentration (Concentration-Time)
$\mathbf{K}_{\mathrm{a}}$	Rate of Absorption
$\mathbf{K}_{\mathrm{cps}}$	Count Rate
$\mathbf{K}_{\mathrm{e}}$	Rate of Elimination
$\mathbf{MRT}_{0-\infty}$	Mean Residence Time of the Drug in Systemic Circulation From Zero to Infinity
$\mathbf{t}_{1/2}$	Half-Life
$\mathbf{T}_{\mathrm{lag}}$	Time Prior to the First Measurable (Non-Zero) Concentration
$\mathbf{T}_{\max}$	Time-to-Peak Concentration
$\mathbf{V}_{\mathrm{d}}$	Volume of Distribution
$\mathbf{V}_{\mathrm{z}}\mathbf{/F}$	Apparent Volume of Distribution After Extravascular Administration
λ_{z}	Apparent Terminal Elimination Rate Constant

Chapter 1

Introduction

1.1 Introduction

Oral medication is the most widely used method of drug administration due to its many benefits, including patient choice, cost-effectiveness, ease of large-scale production of oral dosage forms, and the convenience of administering drugs orally. The oral route is used to administer around 60% of well-known small-molecule medicinal products that are sold commercially. Oral formulations account for over 90% of the worldwide market share among all pharmaceutical formulations meant for human consumption [1].

Compared to parenteral routes, including intravenous, subcutaneous, and intramuscular injections, and the inhalation route for asthma treatments, patients typically comply better with oral formulations [2]. Additionally, medications taken orally can be directed to specific areas of the gastrointestinal (GI) tract to treat pathological conditions like colorectal and stomach cancers, infections, inflammations, bowel diseases, gastro-duodenal ulcers, and gastro-oesophageal reflux disorders locally [1]. (Figure 1.1)

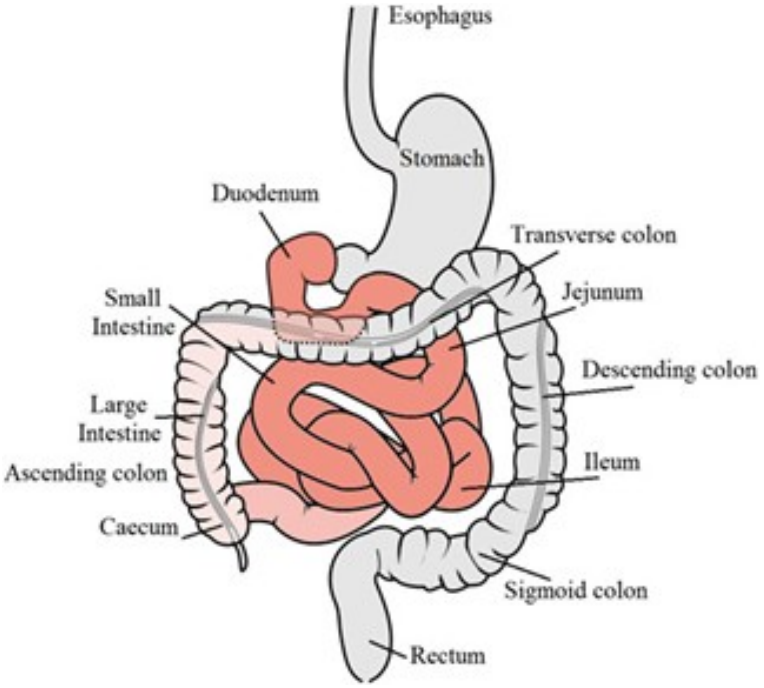

FIGURE 1.1: Gastrointestinal tract showing the major regions for drug absorption denoted in red color. [1]

Notwithstanding these benefits, several difficulties in formulating and administering the oral formulations are mostly related to the physicochemical characteristics of medications, such as their low water solubility and membrane permeability. Drug low chemical and biological stability and GI physiological obstacles, including pH, efflux transporters, and metabolic enzymes, can also impede absorption. Additionally, certain medications may result in nausea and physical discomfort [3].

The duodenum and jejunum in the upper GI tract are principally responsible for the absorption of the majority of drugs taken orally (Figure 1.1). Due to the stomach's smaller surface area and thicker mucus layer (thickness, 1.5 mm), it has a lower capacity to absorb drugs than the intestine [4].

Some obstacles to drug absorption in the GI tract exist in the intestinal epithelium. While the microvilli significantly expand the surface area available for absorption in the small intestine, they also act as an enzymatic barrier since digestive enzymes are concentrated along their brush boundary [5].

Intestinal metabolism is often initiated by digestive enzymes secreted by the pancreas, such as lipases, amylases, and peptidases, including chymotrypsin and trypsin, as well as those originating from the intestinal microflora of the colon, primarily located in the lower part of the GI tract. Enzymes found in the brush border membrane also facilitate first-pass metabolism, which comprises intracellular and brush-border metabolism, on the surface of enterocytes. Small intestinal metabolism is the primary site of brush-border metabolism. Alkaline phosphatase, sucrose, isomaltose, and other peptidases are involved in the metabolism of the brush boundary. First-pass metabolism limits drug absorption to some extent [6].

Drugs need to be released from the dosage form to be absorbed in the GI tract; the released drug dose must be in a solution form or be soluble in the GI fluid. The dissolved medication also needs to be able to pass through the intestinal barrier.

Consequently, the Biopharmaceutical Classification System divides medications into four groups based on the water solubility and intestinal epithelial membrane permeability of the pharmaceuticals, which are the key factors influencing GI absorption [7].

1.2 Biopharmaceutics Classification System

It is an essential framework developed by the FDA to categorize drugs based on their solubility and permeability. This classification is instrumental in predicting a drug's bioavailability when administered orally. The BCS categorizes drugs into four classes, focusing on intestinal permeability, aqueous solubility, and dissolution rate, collectively determining the absorption of active pharmaceutical ingredients (APIs). These factors are critical determinants of the efficacy of oral drug formulations, offering a structured framework for the optimization of drug design and delivery strategies [8].

Permeability is often referred to as the diffusion across the apical membrane of enterocytes into the cytosol, and it depends on drug properties such as polarity, charge, and lipophilicity [10]. If 90% of the prescribed dose is absorbed, the

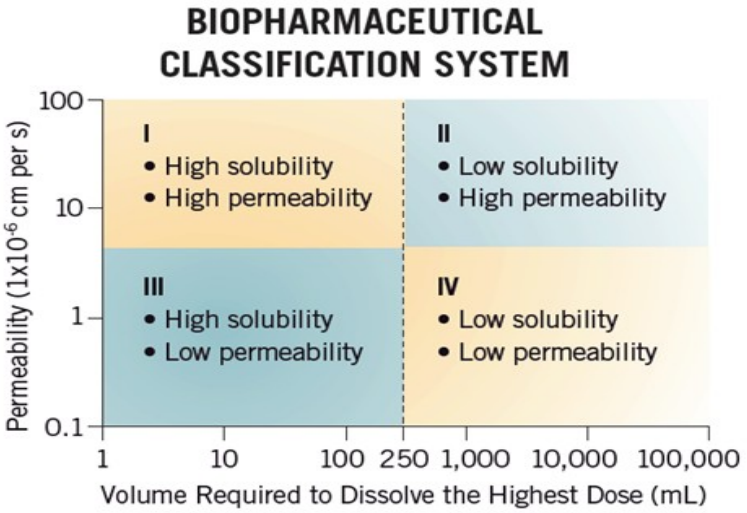

FIGURE 1.2: The Biopharmaceutical Classification System of drugs [9]

drug is considered extremely permeable. BCS Class I medications are excellent choices for oral administration due to their high permeability and solubility. On the other hand, some drugs are difficult candidates for oral delivery because of their low solubility (BCS Class II), low permeability (BCS Class III), or both low solubility and low permeability (BCS Class IV). Increasing the dissolution rate of BCS Class II drugs can enhance their oral absorption capacity [11]. It is important to comprehend the limitations while developing oral formulations for drugs that have low water solubility. One important factor contributing to hydrophobic drugs poor oral bioavailability is their solubility [12].

Bioavailability refers to the rate and extent to which an active drug reaches its intended biological site [13]. Food impact, gastrointestinal discomfort, delayed beginning of action, lack of dosage proportionality, and substantial intra- and inter-subject variability are additional factors associated with reduced bioavailability of hydrophobic medicines. Thus, many strategies are being used to increase the drugs' aqueous solubility [14].

1.3 New Oral Drug Delivery Techniques

New oral drug delivery techniques have been made possible by the exponential growth of nanotechnology. Oral drug delivery systems have been produced using

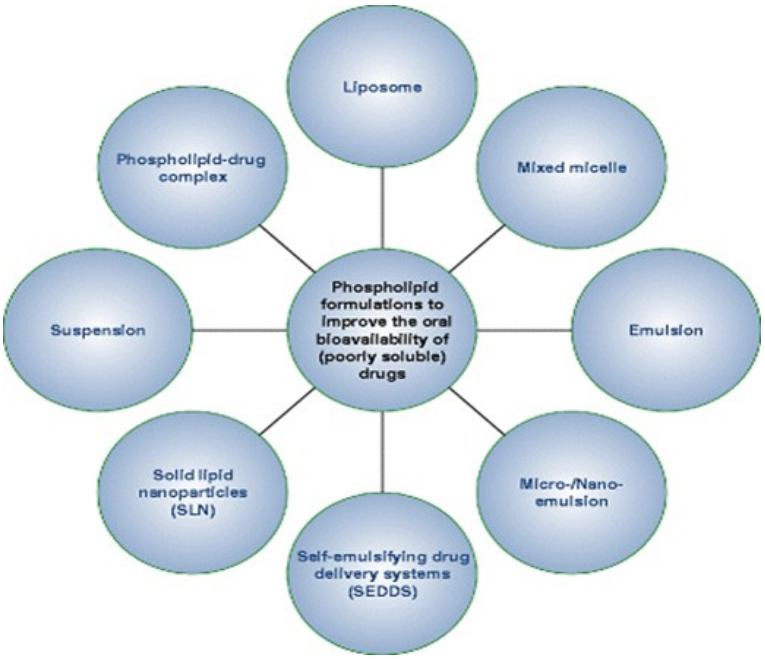

FIGURE 1.3: Various strategies for enhancing oral drug delivery systems [14]

a variety of polymers, both natural and synthetic. Dextran, chitosan, gelatin, and alginate are examples of typical natural polymers, whereas polylactide-coglycolide (PLGA), polylactide (PLA), polycaprolactone (PCL), polyglycolide, polycyanoacrylate, and polyaziridine are examples of synthetic polymers used as oral drug delivery vehicles or carriers [15]. Utilizing particles in the 10–1,000 nm size range, drugs are formulated by the nanotechnology technique. Nano-carriers can be made in two groups using a variety of techniques:

1.3.1 Top-down Techniques

This method of nanoparticle fabrication, commonly referred to as a top-down approach, involves the mechanical breakdown of larger polymeric structures into nanoscale particles using various high-energy techniques. These include high shear mixing, ultrasonication, cavitation, homogenization, microfluidization, spray drying, and milling. Each of these processes applies physical force to disintegrate bulk materials into smaller fragments, ultimately resulting in uniform nanosized particles. For instance, ultrasonication uses high-frequency sound waves to create microbubbles that collapse and produce intense energy, while high-pressure homogenization forces the material through narrow gaps to achieve particle size

reduction. These techniques are widely utilized due to their effectiveness in producing stable nanoparticulate systems with controlled size distribution, which is essential for enhancing the solubility, dissolution rate, and bioavailability of poorly water-soluble drugs [16].

1.3.2 Bottom-up Techniques

They are typically referred to as phase separation techniques and are based on the growth of particles created from individual particles. Pharmaceutical technologies based on supercritical fluid, coordinated crystallization during freeze-drying, and spray-freezing liquid are a few examples [17].

Drug solubility and dissolution rate are eventually improved when particle sizes are reduced to the nanometer scale because this increases the effective surface area [18]. Polymeric nano-carriers can be utilized to transport insoluble medications, direct the medications to certain areas of the gastrointestinal tract, reduce the impact of food on drug absorption, enable receptor-mediated intracellular drug administration, and ease the transcytosis of medications across mucosal membranes [18, 19]. The ability of micro/nano-carriers to transport a broad range of agents for diagnosis and treatment, including tiny molecules, peptides, proteins, and nucleic acids, and to release them in a regulated manner, is another characteristic that makes them effective oral medication carriers. The specificity, tolerability, and effectiveness of medicinal agents can therefore be improved via polymeric nano-carrier based drug delivery [1].

1.4 Loperamide

LPM classified as a BCS Class II drug, is an over-the-counter drug that helps people control their symptoms of diarrhea by improving fluid absorption, lowering intestinal transit, and reducing fluid production. LPM is an opioid receptor agonist, pharmacologically LPM peripherally acting -opioid receptor (-OR) agonist, which reduces gastrointestinal motility and enhances fluid reabsorption [21].

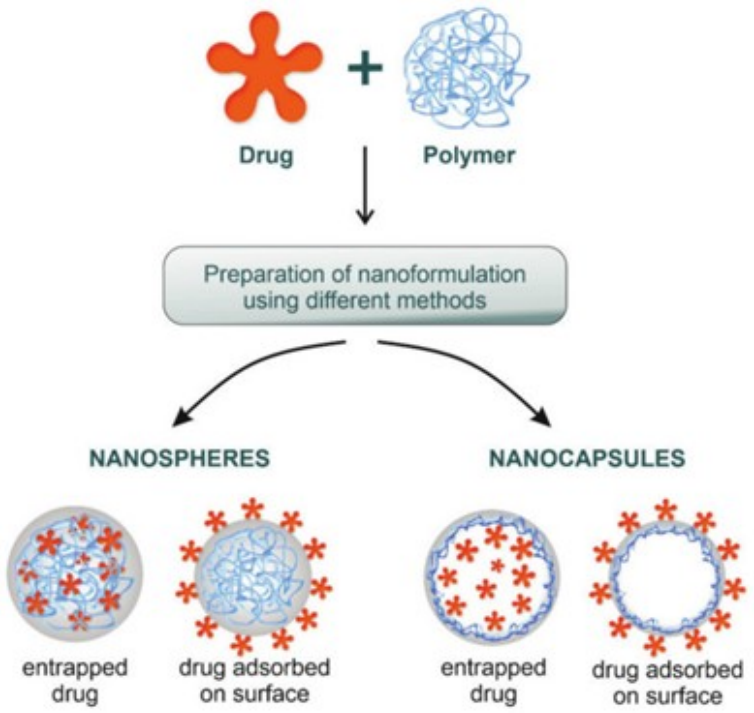

FIGURE 1.4: Types of Nano-Formulations [20]

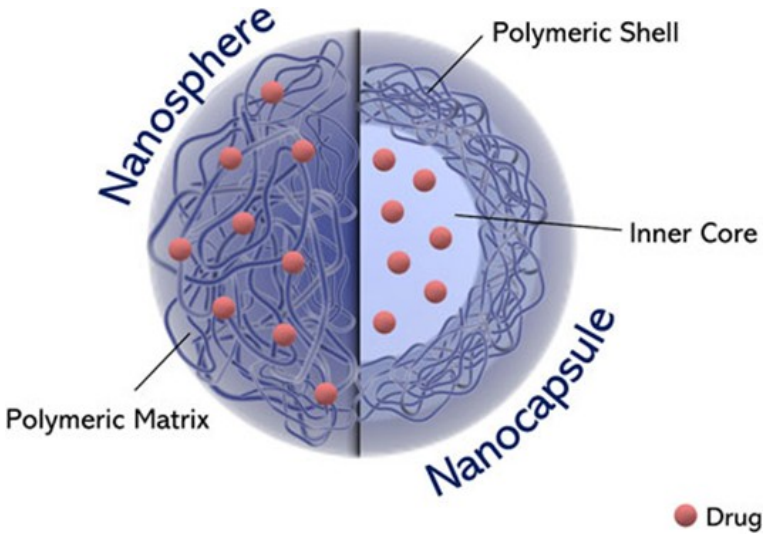

FIGURE 1.5: Structure of a Nano-carrier with encapsulated drug[20]

LPM decreases gastrointestinal motility in both humans and animals. In isolated-organ tests, LPM suppressed the spasmogenic effects of prostaglandins, nicotine, and electrical stimulation while also causing a dose-related decrease in the pressure-induced activity of the ileum's longitudinal and circular muscles. LPM is more effective than diphenoxylate, morphine, or codeine at reducing castor oil-induced diarrhea in rats and mice, as well as the gastrointestinal progression of a charcoal bolus in mice.

Unlike diphenoxylate, oral doses (2.5 to 40 mg/kg) several times the antidiarrheal dose do not have narcotic-like effects. However, high subcutaneous doses of LPM (40–240 mg/kg) or intravenous dosages (0.1 mg/kg) may cause opiate agonist action. Unlike diphenoxylate, LPM has no analgesic effects with non-toxic oral dosages [22].

The plasma half-life in humans is 7 to 15 hours, and peak plasma levels happen 4 hours after ingestion. One to two percent of an oral dosage is eliminated in the urine as free drug or glucuronic acid conjugate, and twenty-five percent is eliminated in the feces unaltered after three days.

Although biliary elimination has not been explored in humans, it is a significant excretion pathway in rats [23]. It seems that LPM is well tolerated.

However, LPM has been associated with dry mouth, rash, dizziness, nausea, and cramping in the abdomen. Around 70% of the administered dose of LPM is readily absorbed from the gastrointestinal (GI) tract; however, due to significant first-pass metabolism, its systemic bioavailability is less than 1%.

This metabolic process substantially limits the amount of the drug that reaches the systemic circulation, thereby reducing its therapeutic efficacy. LPM's low water solubility is a critical physicochemical characteristic contributing to its poor oral bioavailability.

The drug's hydrophobic nature results in a slow dissolution rate in the aqueous environment of the GI tract, which limits its availability for absorption across the intestinal epithelium. These combined factors significantly reduce bioavailability [24].

To address the bioavailability issue, various nano-carriers such as liposomes [25], polymeric nanoparticles, and solid lipid nanoparticles (SLNs) [24]. , Nano lipid carriers (NLCs), nanocrystals, micelles, Niosomes, and Nano emulsions offer effective ways to enhance the bioavailability of LPM.

These nanocarriers improved the absorption, stability, and solubility of drugs, leading to better therapeutic outcomes and reduced side effects [26].

1.5 EUDRAGIT® L 100

It is a pH-sensitive anionic copolymer of methacrylic acid and ethyl acrylate widely used as a drug carrier to enhance oral bioavailability by ensuring drug release in the intestine while protecting drugs from gastric degradation and first-pass metabolism. Its enteric coating properties allow dissolution at pH > 6, enabling site-specific delivery in the jejunum, where drug absorption is optimal. Studies demonstrate its effectiveness in formulations like nanoparticles and microspheres, where it improves drug stability, solubility, and therapeutic outcomes. Eudragit® L 100 is a versatile polymer that enhances and improves the pharmacokinetic profile and bioavailability of drugs having low oral bioavailability [27]. The pharmacokinetic profile and bioavailability will be improved by encapsulating LPM in Eudragit® L 100 Nanoparticles. Conventional LPM formulations need higher doses due to their poor solubility and significant pre-systemic metabolism, which might produce systemic side effects. LPM-loaded Eudragit® L 100 Nanoparticles (LPM-L-E NPs) protect drugs from gastric degradation and early metabolism by releasing the LPM in the intestine [20].

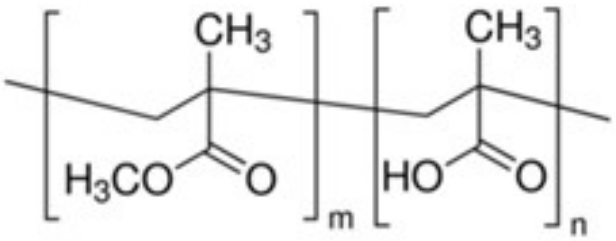

FIGURE 1.6: C hemical structure of Eudragit L-100 (Polymethacrylic acid, Methyl methacrylate – 1:1)[20]

1.6 Aims

Formulation and characterization of pH-sensitive LPM-L-E NPs to improve the solubility, bioavailability, and pharmacokinetic profile of the LPM drug.

1.7 Objectives

Preparation and optimization of LPM nanoparticles.

Physicochemical & in vitro characterization of LPM-L-E NPs.

In vitro drug release studies

In vivo bioavailability studies of LPM-L-E NPs

Chapter 2

Literature Review

The study by Ueda, Iwara, and Kreuter (1998) investigates how different preparation methods affect the drug release behavior of LPM-loaded nanoparticles. Using low molecular weight polylactic acid (PLA) and polylactic-co-glycolic acid (PLGA) as carriers, the researchers compared two nanoparticle formulation techniques: incorporation and adsorption.

In the incorporation method, LPM and polymer were co-dissolved in an organic solvent, and sorbitan fatty acid esters (SFAEs) were added to enhance drug entrapment. The adsorption method involved adding LPM in methanol to preformed nanoparticles at various stages of solvent removal, with adsorption data fitting well to a Langmuir isotherm. Both methods produced high drug loading when low molecular weight polymers were used, and while SFAEs significantly improved entrapment in the incorporation method, they did not affect adsorption capacity.

Drug release from the nanoparticles followed a biphasic pattern in all cases, an initial burst followed by a slower, sustained phase. Without SFAEs, both methods have comparable release profiles, but when SFAEs were included in the adsorption process, the extent of drug release increased. The study concludes that low molecular weight PLA/PLGA nanoparticles are effective for high loading and rapid release of lipophilic drugs like LPM, and that the combination of adsorption with surfactants such as SFAEs can further optimize the release profile [28].

Wei L and his team (2016), developed and evaluated two solid lipid nanoparticle (SLN) formulations loaded with LPM using Dynasan114 (glyceryl Tri myristate) and sodium cholate via a modified solvent evaporation method, aiming to improve oral absorption for diarrhea treatment. They prepared two versions LPM SLN 1 with a high lipid-to-drug ratio (∼303 nm) average size, 87% encapsulation efficiency) and LPM SLN 2 with a lower ratio (∼519 nm, 84% encapsulation) both spherical and smooth under electron microscopy. In vitro release studies showed a steady, sustained drug release without an initial burst.

Significantly, in vivo pharmacokinetic tests in Wistar rats revealed that LPM SLN 1 boosted oral bioavailability to about 227% of that of standard LPM tablets, while LPM SLN 2 achieved 153%, yet maintained similar time-to-peak concentration ($T_{\max}$) as the tablet. The authors concluded that these SLN formulations, particularly the high-lipid variant, represent promising carriers for enhancing the oral delivery and therapeutic efficacy of poorly water-soluble drugs like LPM [24].

Yadav and team (2024), reported the development of a Tween80-coated chitosan nanoparticle formulation encapsulating LPM hydrochloride (LH) designed to enhance blood-brain barrier (BBB) penetration and induce neurotoxic effects in mice. Using a 3^2 factorial design, they optimized nanoparticles with sizes ranging from 189 to 278nm and drug entrapment efficiencies of 80–89%. Administered orally at 1mg/kg for 15 days, LPM chitosan NPs (LCNP) but not free LH elicited psychosis-like behaviors in mice, including increased stereotypy, hyperlocomotion, prolonged immobility, and greater step-down latency. Biochemical assays revealed that LCNP treatment significantly reduced brain glutathione (GSH) and GABA levels and elevated malondialdehyde (MDA), signaling oxidative stress. Histopathologically, LCNP caused cortical neuronal damage, marked by perinuclear vacuolization and hyperchromatic nuclei. The study concludes that Tween80-modified chitosan nanoparticles effectively enhance LH delivery to the brain and provide a valid chemical model for psychosis, with strong face, predictive, and constructive validity [21].

To overcome drug intrinsic issues of poor water solubility and substantial first-pass metabolism, Choudhary AK and his team (2025) investigated the formulation of

LPM nanocrystals to improve its pharmacokinetic profile in a preclinical veterinary model employing Wistar rats. With a mean particle size of 168.4 ± 3.9 nm, a polydispersity index of 0.192, and exceptional colloidal stability demonstrated by a zeta potential of 28.1 mV, the nanocrystals were created via anti-solvent precipitation and refined for stability and homogeneity. Solubility experiments supported this formulation achievement by demonstrating a noteworthy 3.4 - 3.7-fold improvement in the rate of dissolution in simulated biological fluids compared to the pure medication. Furthermore, a longer half-life and mean residence time were indicators of a prolonged systemic exposure in the group treated with nanocrystals. Histopathological studies revealed less gastrointestinal damage, and the formulation maintained a 60% survival probability over 14 days, further confirming the safety profile. This study effectively highlights how nanocrystal technology can greatly improve the therapeutic efficacy and safety of LPM [29].

Eudragit® polymers have been widely employed in drug delivery systems aiming to improve oral bioavailability, especially for drugs with poor aqueous solubility or that were susceptible to degradation in the stomach. Different grades of Eudragit® had been selected depending on desired pH sensitivity, release profile, or site-specific targeting. The study prepared and optimized Eluxadoline-loaded Eudragit® nanoparticles by using a solvent evaporation method. The optimized formulation had a particle size of about 286 ± 3.67 nm, PDI ≈ 0.263, and zeta potential 31.8 ± 3.18 mV. In vitro release studies showed that Eluxadoline-loaded Eudragit® NPs provided sustained drug release; most of the drug was released at pH 6.8 rather than in acidic (pH1.2) medium, indicating that the Eudragit® polymer protected Eluxadoline from the stomach environment and released it predominantly in the intestine [20].

Eudragit® S100 was used as an enteric coating for PLGA-NPs loaded with Etoricoxib to enable colon-specific drug delivery. The coating significantly reduced drug release in acidic and early intestinal pH, ensuring minimal release in the stomach and small intestine. In human pharmacokinetic studies, the Eudragit® coated formulation delayed the time to peak concentration, extended the drug's residence time, and enhanced oral bioavailability by over fourfold compared to the standard

tablet. This demonstrated Eudragit®'s effectiveness in protecting the drug from premature release and targeting delivery to the colon [30].

LPM-loaded nanocarriers were developed and characterized via the nano-precipitation method using ammonium methacrylate copolymers and poloxamer 188 to enhance oral bioavailability and to achieve high encapsulation efficiency (93%) by adjusting the aqueous phase pH. Diafiltration was employed to separate encapsulated from free drug, revealing that approximately 38% of the drug was reversibly bound and 62% irreversibly bound to the nanocarriers. This mechanistic approach provides insights into drug-nanocarrier interactions and supports the design of optimized nanocarrier systems for enhanced drug delivery [31].

Eudragit RS (ERS) nanocarriers coated with poloxamer 188 (P188) were developed to enhance the cellular uptake and transepithelial transport of LPM, a μ-opioid agonist with poor gastrointestinal absorption due to low solubility and P-glycoprotein (P-gp) efflux. P188 was selected for its P-gp inhibitory properties, while ERS improved aqueous dispersibility. Using MDCK-hMDR1 cells, the study found that P-gp limited LPM uptake, and preincubation with P188 significantly increased uptake compared to coincubation. The ERS/P188 nanocarriers enhanced both uptake and absorptive transport of LPM. Additionally, pharmacological P-gp inhibition during transport assays suggested that the unstirred water layer (UWL) might obscure P-gp effects. These findings support the nanocarrier system as a promising strategy to improve LPM bioavailability and analgesic efficacy [32].

The goal of the study was to create a new, environmentally friendly core-shell nanoparticle system for the oral administration of enoxaparin, a potent anticoagulant with limited gastrointestinal absorption. Without the use of organic solvents or high-energy homogenization, the Eudragit® L100 coated chitosan core shell nanoparticles (Eud/CS/Enox NPs) were successfully produced. With a particle size of less than 300 nm, a polydispersity index of roughly 0.12, a zeta potential of more than +25 mV, and a high entrapment efficiency above 95%, the resultant spherical nanocarriers were extremely stable and homogeneous [33].

Chapter 3

Methodology

3.1 Study Setting

The current investigation was carried out from February 2025 to July 2025 in a postgraduate research lab at Capital University of Sciences and Technology and the QC lab of Davis Pharmaceutical Laboratories, Islamabad.

3.2 Animal Study Design

A concurrent quantitative approach was employed in the study. Normal saline, LPM-L-E NPs, and pure drug of LPM were given to the group of healthy rats divided into three groups. The in vivo pharmacokinetic study was structured using a three-group design to evaluate and compare the performance of the developed nanoparticle formulation. Group I served as the control group and was administered normal saline to establish baseline physiological parameters. Group II represented the positive control group, which received the conventional LPM suspension, allowing for a comparison against the standard drug delivery method. Group III, designated as the test group, was administered the optimized LPM-L-E NPs. This design facilitated a direct assessment of the pharmacokinetic improvements offered by the nanoparticle system in contrast to the traditional suspension

form and provided a clear understanding of its therapeutic potential in a biological setting. These were present in the animal house of the university.

3.3 Materials

The LPM was sourced from Davis Pharmaceutical Laboratories, Islamabad. Eudragit® L 100 was procured from Evonik, Germany, while Polyvinyl Alcohol (PVA) and Dichloromethane were both obtained from Davis Pharmaceutical Laboratories, Islamabad. Analytical-grade chemicals and reagents were used throughout the experiment.

3.4 Criteria for Inclusion and Exclusion

The validity and reproducibility of the pharmacokinetic (PK) analysis depend on these inclusion and exclusion criteria. A sample has been taken from rats administered with pure LPM suspension and the LPM-L-E NPs formulation, with the dosage precisely scaled by body weight, in order to be included in the final data set. Additionally, the blood sample needs to have been drawn at one of the exact pre-established intervals (1, 2, 4, 6, 8, 24, 36, or 48 hours after oral administration) and centrifuged effectively to extract the plasma. Lastly, examination of the plasma must have produced a measurable and trustworthy drug concentration value. On the other hand, samples will be excluded if the administration or dosage was incorrect, if the sampling period did not follow the protocol, or if the plasma separation procedure was unsuccessful. Following these guidelines guarantees that only excellent, methodologically sound data are used for the PK modelling that follows.

3.5 Equipment

High-Performance Liquid Chromatography (HPLC Agilent 1220), Dissolution Apparatus (GUOMING RC-6), Homogenizer, Attenuated Total Reflectance Fourier

Transform Infrared (ATR-FTIR) (Bruker alpha), X-ray Powder Diffractometer (XPRD), Scanning Electron Microscope (SEM), and Zeta Sizer were used.

3.6 Method

To prepare LPM-L-E NPs, the initial step involved dissolving 10 mg of LPM and Eudragit® L 100 in 10 mL of Dichloromethane, resulting in the formation of the organic disperse phase (Solution A). In a separate procedure, PVA was dissolved in 20 ml of deionized water to form the aqueous continuous phase Solution (B). Solution (A) was gradually introduced into Solution (B), and the combination is homogenized using a homogenizer to facilitate the formation of nano-sized droplets of the organic phase within the aqueous phase. After homogenization, the mixture was continuously stirred to promote solvent diffusion and evaporation, leading to the creation of LPM-L-E NPs, as dichloromethane had been evaporated. The LPM-L-E NPs were then subsequently collected through centrifugation and freeze-dried to remove any residual moisture, thereby stabilizing the formulation. In the end, the freeze-dried NPs were placed in sealed vials for subsequent evaluations. Optimization of particle size, polydispersity index (PDI), and zeta potential were performed to achieve the desired characteristics for stability and drug release of the nano-formulation [34].

3.7 Physicochemical and In-Vitro Characterization of LPM-L-E NPs

3.7.1 Particle Size Distribution and Polydisperse Index

When defining Nanoparticles (NPs), particle size is a crucial consideration. Additionally, PDI is a measure of the heterogeneity of the sizes of molecules or particles in a mixture, and values larger than 0.5 suggest aggregation of the particles. Particle size is one of the most significant features that affects the in vivo fate of

NPs and dictates the rate and degree of drug release. Dynamic light scattering (DLS) or laser diffraction and Zeta sizer 3000HS (Malvern Instruments, UK) was used to perform these analyses in triplicate. The suspension of Nanoparticles was diluted in distilled water and examined at 25°C before measurement. Every measurement was taken three times to guarantee accuracy. It establishes the surface charge, which is essential for suspension stability. Good stability is indicated by zeta potential values of ±30 mV or greater [30]. The shape and surface properties were determined by the morphological analysis carried out using Scanning Electron Microscopy (SEM), guaranteeing even and smooth coatings [35].

3.7.2 Drug Encapsulation

After centrifugation at 14,500 rpm for 20 minutes, the supernatant was estimated to quantify the drug encapsulation (%DE) in LPM-L-E NPs. The material in the filtrate was then quantified using the HPLC technique. Quantification of LPM NPs using HPLC involves dissolving or digesting the Nanoparticles in a suitable solvent, such as methanol, acetonitrile, or an acidic buffer, to release the encapsulated drug. The solution was then filtered through a 0.22 µm or 0.45 µm membrane to remove particulate matter, followed by dilution with the mobile phase to bring the concentration within the linear range of the HPLC method [24]. A standard solution of pure LPM hydrochloride was prepared in the same solvent or mobile phase to construct a calibration curve. Chromatographic conditions included a C18 column (150 mm × 4.6 mm, 5 µm), a mobile phase of acetonitrile and a buffer (e.g., phosphate buffer, pH adjusted to 3.0–4.5 with phosphoric acid), a flow rate of 0.8–1.5 mL/min. UV detection at 219 nm, and an injection volume of 20–50 µL. System suitability parameters, such as resolution, tailing factor, theoretical plates, and repeatability, were verified before analysis. The LPM concentration was determined by comparing the peak area of the sample with the calibration curve, with adjustments made for any dilution factor and the weight of NPs analyzed. Encapsulation efficiency was determined by comparing the amount of drug encapsulated in the NPs to the total drug used, while drug loading was calculated by comparing the amount of drug in the NPs to their total weight. By dividing the

quantity of drug encapsulated in the NPs by the quantity added to form the NPs, the percentage DE was calculated. The experiment was conducted three times. [9]

$$\% \text{ Encapsulation efficiency } = \frac{\text{Total drug} - \text{Free drug}}{\text{Total drug}} \times 100 \tag{3.1}$$

The loading efficiency was calculated by

$$L(\%) = \frac{Q_n}{W_n} \times 100 \tag{3.2}$$

Qn = Quantity of drug encapsulated

Wn = Total weight of nanoparticles

3.7.3 ATR-FTIR

ATR-FTIR spectroscopy is a versatile analytical method known for its high chemical specificity, providing both qualitative and quantitative insights [36]. It has been widely used in industry and research to analyze various materials, including complex mixtures. The technique enables the study of chemical reactions in solutions, even in aqueous environments. ATR-FTIR also allows for the investigation of reaction kinetics, making it invaluable for understanding chemical processes [36].

3.7.4 X-Ray Powder Diffractometer

The most accurate analytical method for both qualitative and quantitative applications is regularly determined using XRPD. XRPD is a method for examining several kinds of trace evidence, including paint, glass, and narcotics. The recommended technique for identifying crystalline impurities, examining finished dosage forms, and tracking morphological changes during the production process is XRPD [37].

3.7.5 Scanning Electron Microscopy Analysis

The surface morphology of the LPM-L-E NPs was examined using SEM with a Zeiss EVO LS10 instrument (Cambridge, UK). Before imaging, the sample was coated with a thin layer of gold using a gold sputter coater to enhance conductivity. The coated sample was then mounted on a sample stub and analyzed under the SEM to obtain detailed morphological images.

3.7.6 In Vitro Drug Release

A dialysis membrane in USP dissolution (USP Apparatus II) was used to measure the rate at which LPM-L-E NPs dissolve. At 37 ± 0.5°C, a known amount of the NPs formulation was suspended in a suitable dissolving media, such as intestinal fluid (pH 6.8) or simulated stomach fluid (pH 1.2). The apparatus was filled with a known number of NPs, and the medium was agitated at 50–100 rpm. Aliquots were taken at predetermined intervals and filtered to remove any undissolved particles. The drug concentration was then measured using HPLC. A release profile was displayed along with cumulative drug release. The experiment was conducted three times to ensure reliability [24].

3.8 In Vivo Pharmacokinetic Studies

For the pharmacokinetic analysis, the male rats (n=7) were split up into three groups.

Group I: The control group was administered normal saline.

Group II: The positive control group received the conventional LPM Suspension.

Group III: The test group received drug-loaded formulation LPM-L-E NPs.

Group I was administered with normal saline, Group II was given LPM suspension (produced by dispersing LPM) orally, and Group III was given the optimized

formulation. The LPM dosage was given to Group II and Group III at an equivalent concentration of 5mg/kg. Blood samples were collected from the tail vein at predetermined intervals of 1, 2, 4, 8, 24, 36, and 48 hours after treatment. The samples were then processed to create plasma, which was then be used for drug measurement. HPLC was utilized in pharmacokinetic investigations to measure the amount of LPM in plasma. At predetermined intervals following medication delivery, plasma samples were obtained and examined to ascertain important pharmacokinetic parameters. The maximum plasma concentration, or Cmax, and the time it takes to attain it, or Tmax, give information about how quickly drugs are absorbed. The trapezoidal rule was used to compute the area under the plasma concentration-time curve (AUC), which represents the total drug exposure over time and is used to evaluate overall bioavailability [38]. The PK Solver program was used to compute the non-compartmental analysis for finding PK Parameters such as area under the plasma concentration-time curve (AUC), Cmax, and Tmax, which represent the total drug exposure over time and were used to evaluate overall bioavailability. For a drug that enters the body by a first–order absorption process, as in the case of Oral Administration, it is distributed in the body according to one-compartment kinetics, and is eliminated by a first-order process, the model can be depicted as follows:

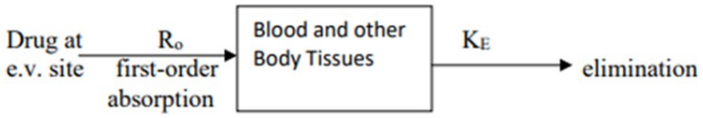

And the Equation used is:

$$C = \frac{K_a F X_0}{V_d \left(K_a - K_e\right)} \tag{3.3}$$

At maximum plasma concentration, the rate of change in plasma drug concentration (dC/dt) is zero, and the rate of absorption is equal to the rate of elimination (Ka.Xa = KEX). This rate is attainable by:

$$K_E \, e^{-K_E t} = K_a \, e^{-K_a t} \tag{3.4}$$

3.9 Statistical Analysis

Statistical analysis of the experimental data was carried out using the GraphPad Prism software, a widely recognized tool for scientific graphing, data analysis, and biostatistics. The data obtained from various experimental groups were expressed as the mean value accompanied by the standard deviation (mean ± SD), which provides insight into the variability and reliability of the data by indicating how much individual data points deviate from the average.

To determine whether statistically significant differences exist among the experimental groups, a one-way analysis of variance (ANOVA) was employed. This test is particularly useful when comparing more than two groups, as it evaluates whether the means of these groups are significantly different from each other. In this study, ANOVA was used to assess the differences in pharmacokinetic parameters, drug release rates, and other relevant outcomes among the control group, the group receiving the conventional LPM suspension, and the group treated with the LPM-loaded nanoparticles LPM-L-E NPs.

If the ANOVA test indicated significant variation among groups, post hoc analyses such as Tukey's test were planned to identify specifically which group pairs differed. This statistical approach ensured that any observed differences in outcomes were not due to random variation but instead reflected the true effect of the nanoparticle formulation. A p-value of less than 0.05 ($p < 0.05$) was considered statistically significant, indicating strong evidence against the null hypothesis and supporting the conclusion that the treatment had a measurable impact.

Chapter 4

Results

4.1 Calibration Curve of Standard LPM Solution and Data Table

A calibration curve is plotted to show the relationship between the concentration of LPM (analyte) and the instrument response (peak area from an HPLC). This

Table 4.1: Concentration of Standard Drug

Nominal Content (%)	Concentration (mg/mL)	Peak Area of Analyte
20	0.1	8102.15
40	0.2	16210.47
60	0.3	24313.75
80	0.4	32416.31
100	0.5	40271.24
120	0.6	48671.12

method helps determine the concentration of unknown samples by comparing them to a standard curve. Nominal Content (%): These are relative concentrations based on a 100% standard. Concentration (mg/mL): It is the actual amount of LPM in solution. Peak Area: It increases as concentration increases, indicating a direct relationship.

4.1.1 Linearity Plot

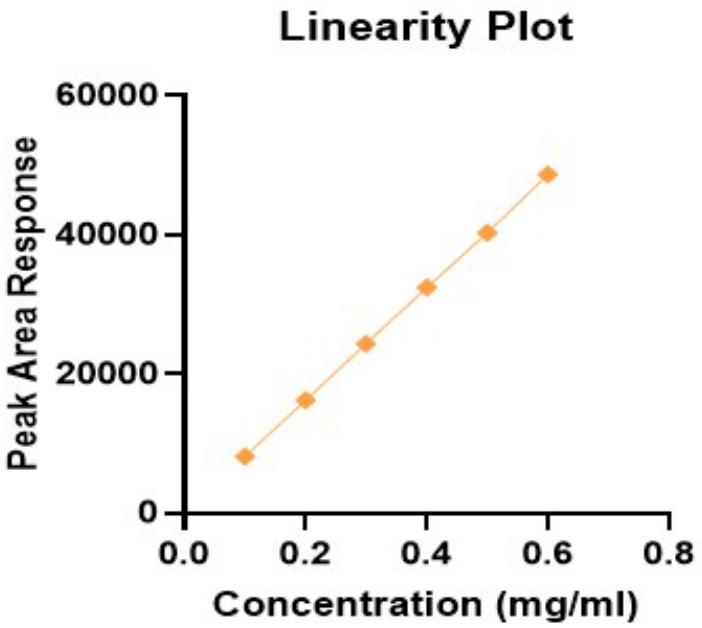

FIGURE 4.1: Calibration Curve of Standard LPM Solution

4.1.2 Linearity Plot Parameter

TABLE 4.2: Linearity plot parameters of Standard LPM

Parameter	**Value**	**Unit / Notes**
Slope (m)	80,894.00	(Peak Area Response) / (mg/mL)
y-Intercept (c)	17.868	Peak Area Response
Correlation Coefficient (R^2)	0.99995	Indicates excellent linearity
Calibration Equation	$y = 80{,}894.00\,x + 17.868$	y: Peak Area, x: Concentration (mg/mL)

This analysis confirms the excellent linearity of the method within the concentration range of 0.1 to 0.6 mg/ml.

The evaluation produced a calibration curve described by the equation y=80,894x + 17.868. This equation highlights a strong sensitivity (indicated by the high

slope of 80,894) and minimal systematic bias (due to the negligible intercept). A correlation coefficient (R2) of 0.99995, approx. to 1, demonstrates a perfect, direct proportional relationship between the analyte concentration (x) and the detector response (y). These results validate the method's suitability for accurate and precise quantitative analysis within the tested range.

4.1.3 Calibration Curve and Method Validation

LPM Hydrochloride (HCl) calibration curve was constructed using HPLC. Its purpose was to establish linearity and validate the analytical method for quantitative determination of LPM HCl.

4.1.4 Method Validation Points

Linearity: Demonstrated over the concentration range 0.1–0.6 mg/mL and a correlation coefficient of 0.99995, indicating perfect linearity.

Sensitivity: High slope value reflects excellent sensitivity, allowing for accurate detection of small concentration changes.

Accuracy & Precision: Data points show a consistent increase with minimal deviation, indicating high reproducibility, and a y-intercept 17.868 indicates minimal background noise or system error.

4.2 Preparation of Plasma Samples and Construction of Calibration Curve for LPM in Plasma & Quantification via HPLC

This section details the comprehensive procedure for preparing plasma samples and generating a calibration curve to quantify LPM using HPLC.

4.2.1 Plasma Sample Collection and Separation

FIGURE 4.2: Plasma Sample Collection and Separation (A, B, C)

Calibration curve in plasma is created from taking from rats in the control group received normal saline. Blood samples were drawn at 1, 2-, 4-, 6-, and 24-hours post-administration. Each sample was immediately transferred to an EDTA tube to prevent clotting and centrifuged at 5000 rpm for 15 minutes at room temperature using a centrifuge. After centrifugation, the plasma supernatant was carefully

transferred to sterile Eppendorf tubes, either for immediate processing or storage at 20 °C.

4.2.2 Plasma Protein Precipitation and Extraction

For LPM extraction, 300 μL of plasma was pipetted into a clean Eppendorf tube. 2 mL of ethanol was added to each aliquot to precipitate proteins and aid drug extraction. The mixture was vortexed for 30 seconds and then centrifuged at 10,000 rpm for 20 minutes. This supernatant, containing the extracted LPM, was carefully decanted into a separate vial. This entire protein precipitation and extraction process was repeated three times for each sample to ensure maximum LPM recovery.

4.2.3 Solvent Evaporation and Reconstitution

The combined supernatants were subjected to evaporation on a hot plate at 40 C to completely remove the ethanol. Once dry, the remaining residue was reconstituted in acetonitrile, which also served as the HPLC mobile phase. The reconstituted solution was briefly vortexed to ensure the LPM fully dissolved.

4.2.4 HPLC Analysis and Calibration Curve Construction

The final, reconstituted solution was filtered and injected into the HPLC system under validated chromatographic conditions. In parallel, a series of LPM standards with known concentrations, prepared in blank plasma using the same method, were analyzed.

A standard calibration curve was generated by plotting the peak area against the LPM concentration for each standard. This curve was then used to assess the method's linearity, precision, and sensitivity in plasma, enabling the accurate quantification of unknown LPM concentrations in future pharmacokinetic studies.

FIGURE 4.3: Sketch-Style Stepwise Workflow Diagram

Schematic Diagram: Plasma Sample Preparation Workflow

[Normal Saline to Control Rats]

↓

[Blood Collection at 1, 2, 4, 24 hrs.]

↓

[Centrifugation at 5000 rpm, 15 mins]

↓

[Plasma Separation]

↓

[300 µL Plasma + 2 mL Ethanol → Vortex]

↓

[Centrifugation at 10,000 rpm, 20 mins × 3]

↓

[Supernatants Combined in Vial]

↓

[Evaporation on Hot Plate at 40°C]

↓

[Reconstitution in Acetonitrile]

↓

[HPLC Run]

↓

[Calibration Curve of Loperamide in Plasma]

4.3 Calibration Curve of Standard LPM Solution in Plasma

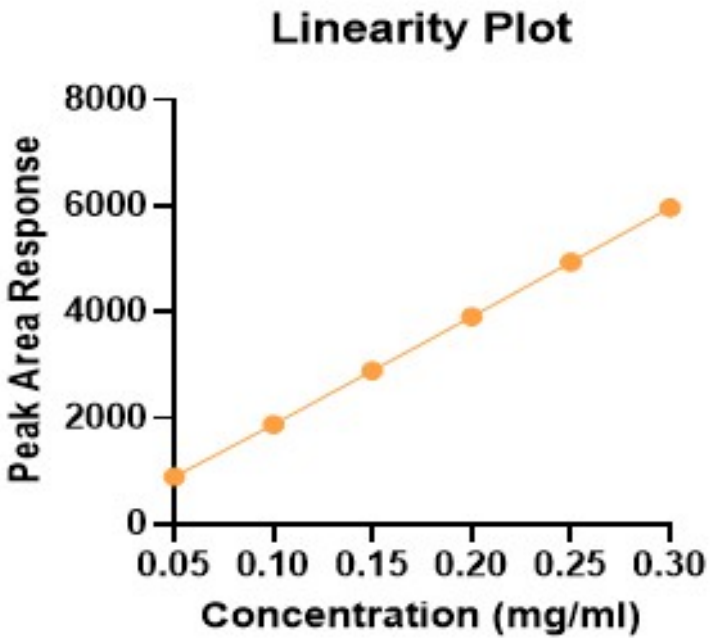

FIGURE 4.4: Calibration Curve of Standard LPM in Plasma

TABLE 4.3: Concentration of standard drug in plasma

Nominal Content (%)	Concentration (mg/mL)	Peak Area of Analyte
20	0.05	898.29
40	0.1	1880.11
60	0.15	2894.62
80	0.2	3918.77
100	0.25	4942.81
120	0.3	5969.33

4.3.1 Linearity Plot Parameter

TABLE 4.4: Linearity plot parameters of LPM in plasma

Parameter	**Value**
Slope (m)	20324.26
Intercept (c)	–139.42
Correlation Coefficient (R^2)	0.9994
Calibration Equation	$y = 2{,}0324.26\,x - 139.42$

The calibration data for LPM HCl demonstrates an excellent linear relationship between concentration (0.05–0.3mg/ml) and peak area response, with a regression equation of y = 20324.26x - 139.42 and an R^2 of 0.9994. The high slope indicates strong method sensitivity, and the negligible intercept shows minimal baseline bias. Overall, the data confirm outstanding linearity and method suitability for quantitative estimation of LPM HCl in this concentration range.

4.4 Particle Size Distribution and Polydisperse Index

NPs must have a small particle size, low PDI, and high ZP values for the effective bio-distribution of a drug. The dynamic light scattering (DLS) analysis of LPM L E NPs revealed a Z-average diameter of 312.3 nm, indicating that the particles fall within the typical nanoparticle size range. The size distribution by intensity displayed a single sharp peak at approximately 330.8 nm, which suggests that the sample contains a uniform population of nanoparticles without significant aggregation. The % intensity for Peak 1 was 100%, confirming the presence of a single, dominant particle population. Furthermore, the polydispersity index (PDI) was 0.109, reflecting an excellent monodispersity and a uniform formulation. The standard deviation of 87.84 nm indicates a moderate yet acceptable spread of

particle sizes around the mean, consistent with a sharp distribution profile. The intercept value of 0.938 and a count rate of 238.9 kcps further support the reliability and quality of the measurement, confirming that the sample preparation and measurement conditions were optimal. Overall, these findings demonstrate that formulation consists of high-quality, monodisperse nanoparticles suitable for pharmaceutical and biomedical applications, such as drug delivery systems, where consistent particle size and stability are critical.

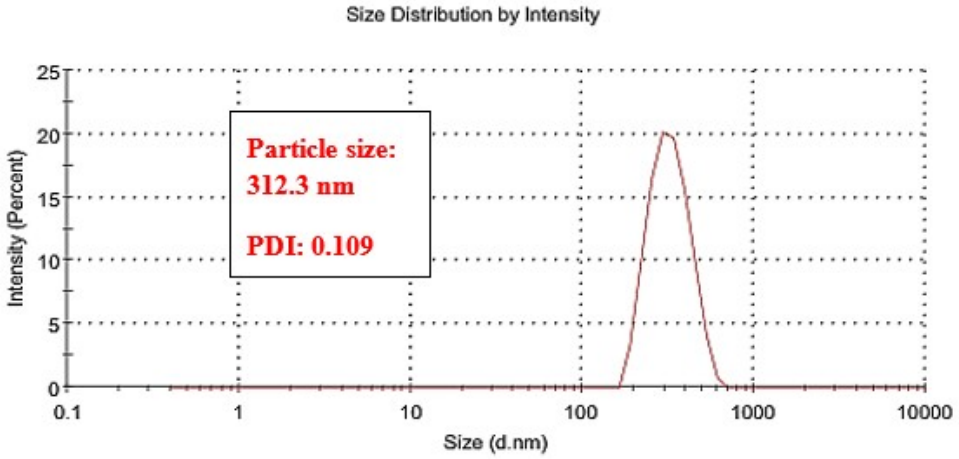

FIGURE 4.5: Particle Size Distribution and Polydisperse Index

LPM-L-E NPs are composed of uniform nanoparticles averaging 312 nm, with an excellent PDI (0.109), indicating high mono dispersity and no aggregation. The high intercept (0.938) and clean intensity distribution confirm strong measurement quality. This sample is deal for biomedical and pharmaceutical applications, including nano-carriers, delivery systems, and diagnostics.

4.5 Zeta Potential

The zeta potential measurement for the LPM-L-E NPs revealed a mean zeta potential of -10.2 mV, as identified from the graph. This single peak distribution indicates a uniform surface charge across the particle population, suggesting that the nanoparticles are relatively stable but may possess moderate electrostatic repulsion. Typically, zeta potential values greater than ±30 mV are considered

TABLE 4.5: Physicochemical characteristics; Particle size and Polydispersity Index (PDI)

Parameter	**Result**	**Interpretation**
Z-Average Diameter (d.nm)	312.3 nm	Hydrodynamic diameter within nanoparticle range; suitable for drug delivery uses.
Peak Size (d.nm)	330.8 nm	Single population detected; uniform size distribution.
% Intensity (Peak 1)	100%	Entire signal from a single size group — no aggregation detected.
PDI (Polydispersity Index)	0.109	Very low PDI; excellent monodispersity and formulation uniformity.
Standard Deviation	87.84 nm	Moderate spread, still acceptable given the sharp peak and low PDI.
Intercept	0.938	Strong signal, confirming good measurement quality.
Measurement Duration	70 seconds	Standard measurement time; data is robust.
Count Rate (kcps)	238.9	Optimal count rate indicating well-prepared sample.
Graph Observation	Single sharp peak	Confirms absence of multiple particle populations or aggregates.

highly stable, whereas values between ±10 mV and ±30 mV indicate incipient stability where some aggregation may occur over time. Therefore, a zeta potential of -10.2 mV suggests that the nanoparticles exhibit stability in suspension, potentially requiring stabilization with surfactants or polymers to prevent aggregation. The absence of additional peaks further supports the presence of a single particle population, reflecting uniformity in particle surface characteristics.

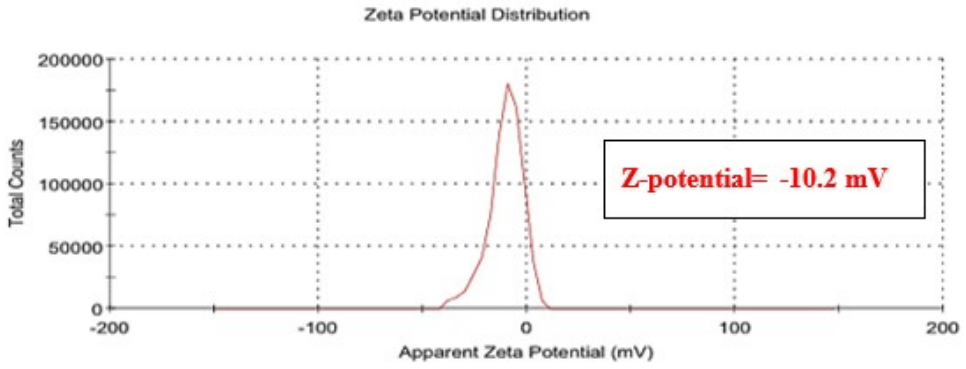

FIGURE 4.6: Zeta Potential

4.6 Drug Encapsulation Efficiency

The % EE was determined by measuring the concentration of free NP in the dispersion medium. NP dispersion was centrifuged at 14500 rpm for 20 minutes. Upon centrifugation, the supernatant was collected, and the procedure was repeated thrice, and the collected supernatant was analyzed for unencapsulated LPM-L-E NPs by HPLC.

The following equation was used to determine entrapment efficiency:

$$\%EE = \frac{M_{\text{initial drug}} - M_{\text{free drug}}}{M_{\text{initial drug}}} \times 100 \tag{4.1}$$

Where "M initial drug" is the mass of initial drug used, and the "M free drug" is the mass of free drug detected in the supernatant after centrifugation. The entrapment efficiency of LPM in the nanoparticle formulation was calculated using HPLC data from standard and sample chromatograms.

The total drug concentration was represented by the peak area of LPM in the standard sample, which was 11024.140. The free (unentrapped) drug was determined by the peak area in the sample, found to be 48.556. Using the formula:

$$\text{Entrapment Efficiency } (\%) = \frac{11024.140 - 48.556}{11024.140} \times 100 = 99.56\% \tag{4.2}$$

The nanoparticle formulation exhibited a very high entrapment efficiency of 99.56%, indicating that nearly all of the LPM was successfully encapsulated. This result suggests strong formulation efficiency and potential for effective drug delivery with minimal free drug presence. The chromatogram [figure 4.7 (a)] shows the HPLC analysis of a sample containing Pure LPM. LPM (standard sample) has a retention period of roughly 1.8 minutes in this system. Good column performance and separation are suggested by the peak's sharpness and symmetry. System stability is indicated by the great reproducibility across replicates. The absence of notable secondary peaks suggests that the sample is pure or effectively isolated from extraneous constituents.

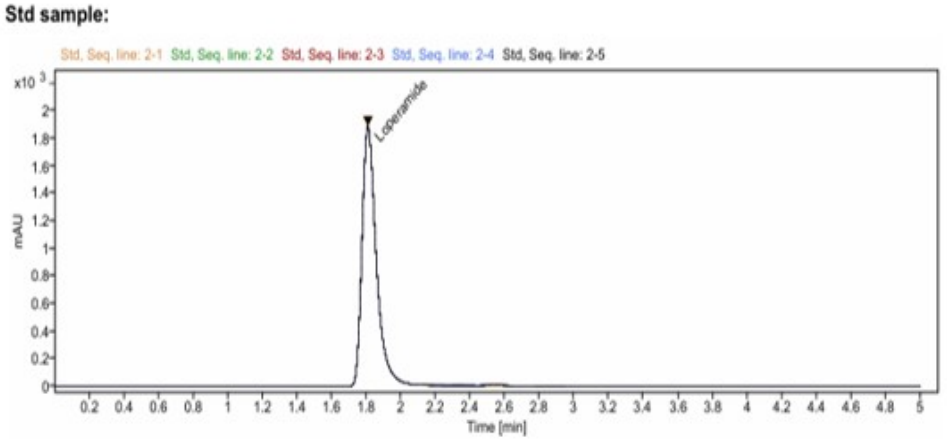

The chromatogram [figure 4.7 (b)] displays two injection runs (orange and green) superimposed on top of an HPLC analysis of a sample containing LPM. The presence of LPM in the sample is confirmed by a strong peak at about 1.8 minutes that corresponds to the retention time seen in the standard chromatogram [figure 4.7 (a)].

In contrast to the pure standard, this graph has extra peaks that show the presence of other chemicals or impurities. Two of these peaks are particularly noticeable at about 1.1 minutes and a wider one between 2.3 and 3.0 minutes. The symmetrical and well-resolved LPM peak indicates dependable detection and strong system performance. Overall, the graph shows that LPM is present in the sample along with other compounds, however there is some fluctuation reflected in the little variations between the two runs in the minor peaks.

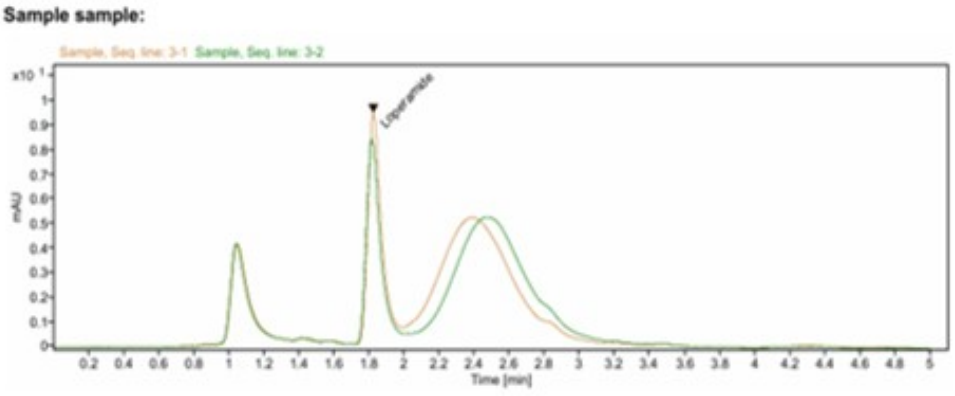

FIGURE 4.7: HPLC Curves to determine drug encapsulation . [(a) standard drug peak (b) drug peak in formulation]

4.7 ATR-FTIR Studies

A comparative ATR-FTIR spectra of pure LPM, L100, PVA, and LPM-L-E (NPs) were studied for the identification of the encapsulated drug inside NPs. The broad O–H band (3309 cm^{-1}) confirms the presence of polyvinyl alcohol (PVA) The C=O stretch at 1718 cm^{-1} is characteristic of ester groups in Eudragit® L100, suggesting successful incorporation into the formulation. The C–H and C–O peaks confirm the organic nature of the polymers used. The characteristic absorption bands of LPM diminished or disappeared in the fingerprint region of the Formulation, which indicated that the drug was encapsulated inside the Eudragit® L100 polymer, and the appearance of new peaks in the formulation corresponding Eudragit® L100 and PVA confirmed successful entrapment. Absence of new peaks indicates no strong chemical interaction (like covalent bonding) between LPM, PVA, and Eudragit® L100, suggesting physical encapsulation. The ATR-FTIR spectrum of the LPM-L-E NPs formulation reveals key absorption bands indicating the successful incorporation and interaction of drug LPM with Eudragit® L100 and other formulation excipients. 2993.14 cm^{-1} and 2951.43 cm^{-1}, these peaks correspond to C–H stretching vibrations typically associated with alkyl groups, indicating the presence of hydrocarbon chains in the polymer backbone (Eudragit® L100) or residual solvent. 2115.19 cm^{-1}, this minor peak may suggest the presence of CC or CN groups, possibly due to structural fragments of the polymer or interactions with PVA. 1704.60 cm^{1}, a strong and sharp absorption band corresponding to the C=O (carbonyl) stretching vibration, a characteristic of ester groups presents in both LPM and Eudragit® L100. These peaks confirm the presence of the drug and polymer [figure 4.8 (a), (b) and (c)].

A band at about 1600 cm^{1} (carboxylic acid group), a high peak at 1720 cm^{1} (ester C=O stretching), peaks at 1250–1150 cm^{1} (C–O–C stretching of esters), and characteristic peaks at 2950–2850 cm^{1} (C–H stretching of alkyl groups) are seen in the FTIR spectra of Eudragit L 100 [figure 4.8 (a)]. The polymer backbone is confirmed by additional peaks in the fingerprint area. These absorptions align with Eudragit L 100's methacrylic acid–methyl methacrylate copolymer structure. The

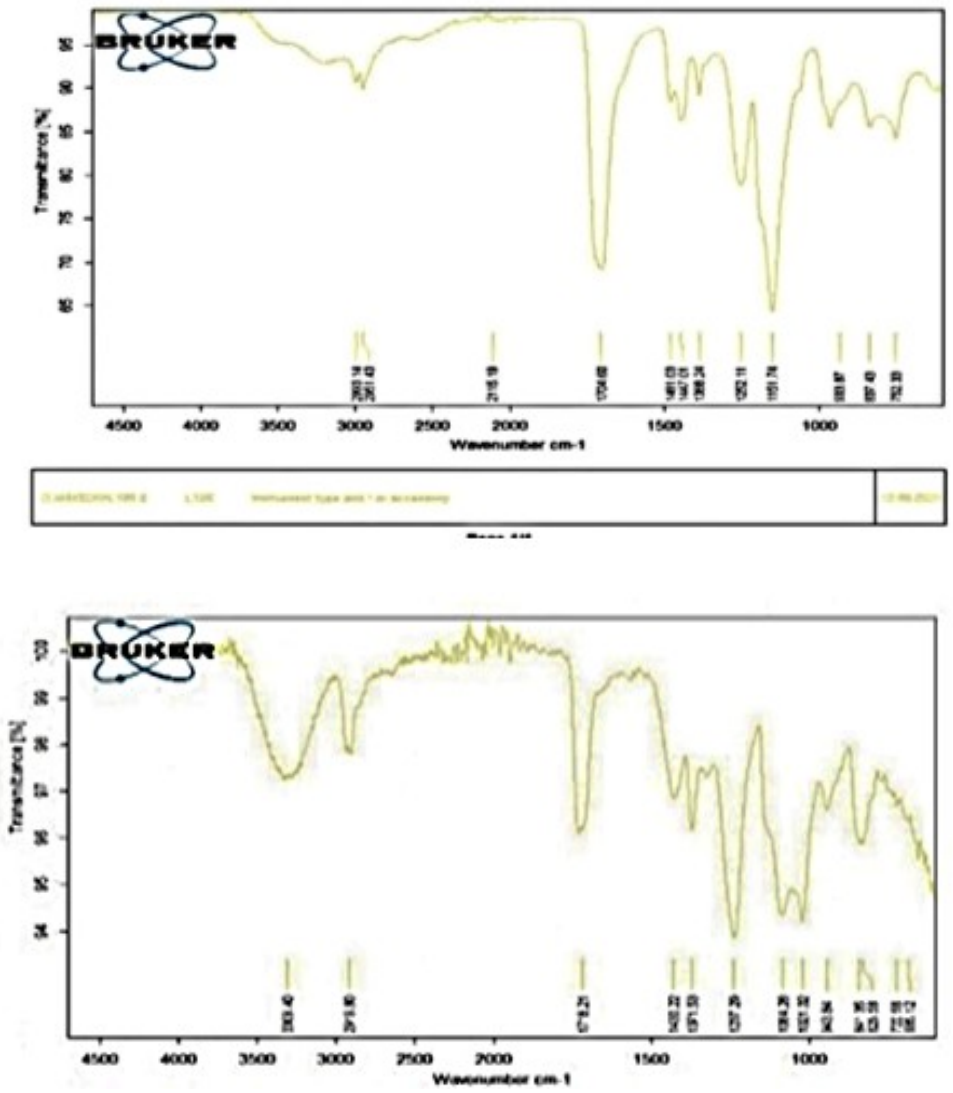

FTIR spectrum [figure 4.8 (b)] exhibits a clear correspondence with polyvinyl alcohol (PVA), a synthetic polymer commonly utilized in nanoparticle formulations due to its hydrophilic nature and excellent stabilizing properties. The spectrum displays a broad and intense O–H stretching band between 3200 and 3500 cm^{1}, indicative of extensive hydrogen bonding among the numerous hydroxyl groups present in the polymer. Smaller C–H stretching peaks are observed in the range of 2940–2850 cm^{1}, corresponding to the methylene backbone of PVA. Additionally, strong C–O stretching, O–H bending, and C–C skeletal vibrations are evident within the 1300–1000 cm^{1} region, which are characteristic of polyalcohol's. A distinct peak around 1140 cm^{1} is also observed, often associated with the crystalline regions of PVA. Overall, the spectrum confirms the chemical identity of PVA, emphasizing its structural integrity and its suitability as a hydrophilic stabilizing

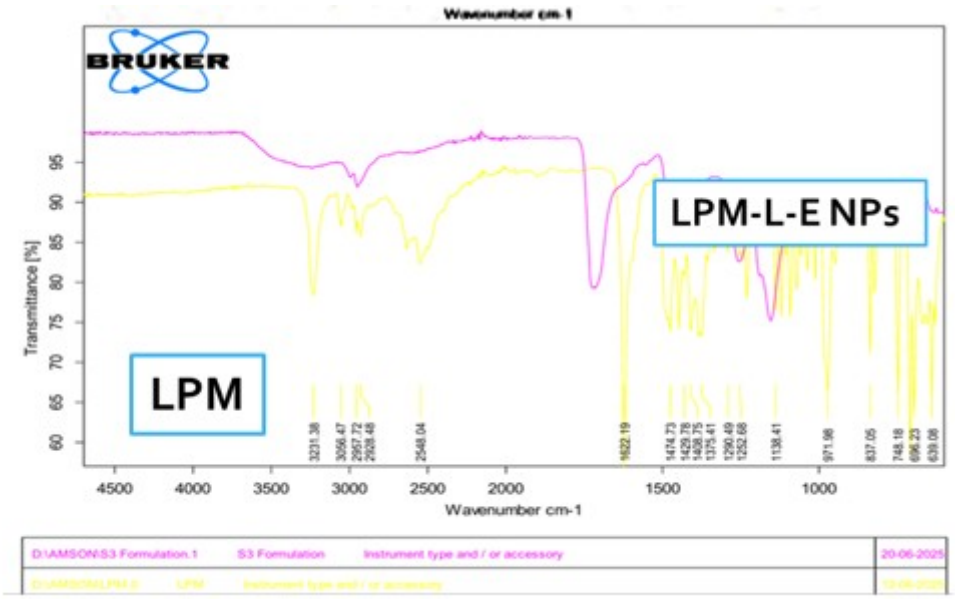

FIGURE 4.8: FIGURE 4.8: FTIR Graphs (a, b & c)

agent in nanoparticle formulations. The FTIR spectrum [figure 4.8 (c)] definitively identifies pure LPM (yellow colour), a synthetic antidiarrheal drug, as it precisely corresponds to the known chemical structure characterized by aromatic rings, amide, ether, and aliphatic functional groups.

The spectrum exhibits a broad N–H stretching band around 3400 cm^{-1} from the secondary amide, indicating potential hydrogen bonding, while distinct C–H stretching peaks at 2920 cm^{-1} and 2850 cm^{-1} confirm the presence of aliphatic methyl and methylene groups. A sharp and prominent C=O stretching peak (amide I band) near 1650–1700 cm^{-1} serves as a defining feature of LPM's amide functionality.

Additionally, a C=C stretching vibration around 1600 cm^{-1} signifies the presence of aromatic rings. The region between 1300–1000 cm^{-1} displays multiple peaks corresponding to C–N and C–O stretching, consistent with ether and amine linkages, while the aromatic C–H out-of-plane bending observed around 750–900 cm^{-1} further supports the existence of aromatic structures. Overall, the FTIR spectrum confirms the chemical identity of pure LPM through its characteristic absorption peaks, and the absence of any unexpected bands indicates its chemical purity and

the lack of degradation or impurities. This FTIR spectrum [figure 4.8 (c)] represents LPM-L-E nanoparticles (pink color), a formulation of LPM encapsulated within Eudragit® L100. The spectrum acts as a chemical fingerprint, blending the signatures of both the drug and the polymer to provide crucial evidence of drug encapsulation and the interactions occurring between them. A broad absorption band around 3400 cm1 indicates O–H or N–H stretching vibrations. This broadening and a slight shift compared to the pure components strongly suggest hydrogen bonding interactions. These likely occur between the hydroxyl groups of Eudragit L100 (or the PVA stabilizer) and the amide group of loperamide, playing a vital role in stabilizing the nanoparticle structure.

C–H stretching peaks are visible near 2920 cm1 and 2850 cm1, consistent with the aliphatic chains found in both loperamide and the polymer. A prominent peak around 1720 cm1 is attributed to the C=O stretching of ester groups from Eudragit L100. While pure loperamide also has a carbonyl stretch in a similar region, the observed single, possibly broader, and shifted peak here suggests overlapping or interaction between the carbonyl groups of the drug and the polymer matrix.

Other expected bands, such as aromatic C=C stretching around 1600 cm1 and the C–N/C–O stretching region between 1250–1000 cm1, are still present but show reduced intensity or slight shifts. This further supports the successful incorporation of loperamide into the polymer network. Similarly, peaks in the 750–900 cm1 range, characteristic of aromatic out-of-plane bending, are preserved, albeit potentially modified, confirming the aromatic rings from loperamide are intact within the formulation.

In conclusion, the FTIR spectrum of LPM-L-E nanoparticles clearly displays the combined characteristics of both LPM and Eudragit L100. The observed shifts and broadenings in key functional group regions provide strong evidence for the successful encapsulation of LPM within the polymer matrix and highlight significant intermolecular interactions, particularly hydrogen bonding, between the drug and the carrier. Importantly, the absence of any new peaks confirms that no chemical degradation or new covalent bonds have formed, thus validating the physical entrapment and compatibility of all components in this nanoparticle formulation.

4.8 XPRD

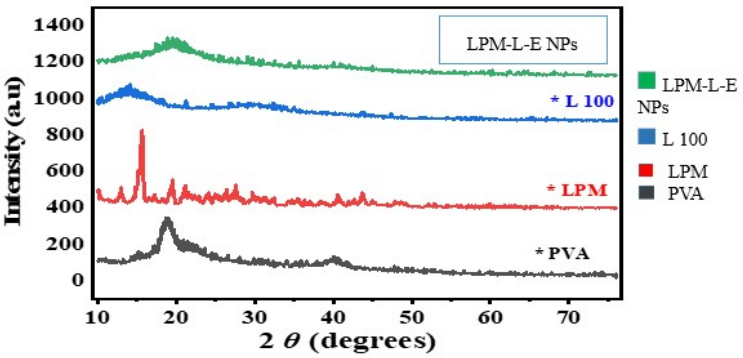

FIGURE 4.9: XRD Graph

This graph displays the XPRD patterns of four different materials, providing insights into their crystalline and amorphous structures. XRD is a powerful technique for material characterization; sharp, intense peaks indicate crystallinity, while broad humps signify an amorphous structure. The graph compares the XPRD patterns of two polymers (PVA and L-100), the active pharmaceutical ingredient LPM, and a formulation (S3). The PVA pattern shows a broad, diffuse hump centered on 220. This indicates that PVA is predominantly amorphous or semi-crystalline. The lack of sharp peaks confirms the absence of a highly ordered crystalline structure. Eudragit L-100 (Blue Pattern) pattern also displays a broad hump, characteristic of an amorphous material. This is typical for Eudragit polymers, which are often used in drug delivery and exhibit high flexibility and a non-crystalline structure. LPM – Red Pattern revealed several distinct, sharp, and intense diffraction peaks (e.g., prominent peaks around 15, 16, and 17) characterize The LPM pattern. These sharp peaks are indicative of crystalline LPM. S3 (LPM-L-E NPs) (Green Pattern) spectra exhibit a broad, diffuse appearance similar to the L-100 and PVA patterns. Crucially, the sharp characteristic peaks of the crystalline LPM are absent or significantly reduced in the S3 formulation pattern.

The XPRD analysis suggests a successful change in the LPM's solid state within the LPM-L-E NPs formulation. The disappearance of the crystalline peaks of LPM in the LPM-L-E NPs pattern indicates that the LPM has likely undergone

an amorphous transition or has been molecularly dispersed within the polymer matrix (L-100 and/or PVA). This amorphous form of LPM in the LPM-L-E NPs formulation is often desirable in pharmaceutical applications as it can significantly enhance drug solubility and bioavailability.

4.9 Scanning Electron Microscope

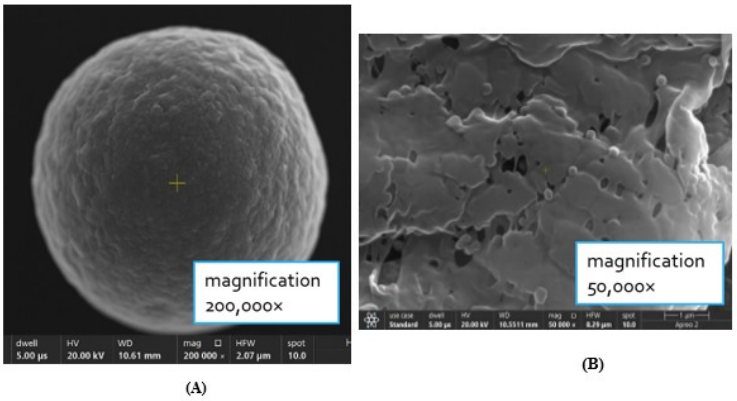

FIGURE 4.10: Scanning Electron Microscope (SEM) images of the formulation (A & B)

This analysis integrates two Scanning Electron Microscope (SEM) images to provide a comprehensive interpretation of the morphology of LPM and L100 nanoparticles. These images highlight different levels of magnification, revealing both the macrostructure of the formulation and the detailed morphology of individual nanoparticles.

The first image Figure 4.8A (magnification 200,000×) provides an ultra-high-resolution view of a single, roughly spherical particle. The particle exhibits a spherical or near-spherical shape. Crucially, the surface is notably rough and granular. It is not a smooth sphere, but appears to be composed of smaller, tightly packed, aggregated subunits. This morphology suggests that the nanoparticle itself is a complex aggregate, possibly composed of LPM nanocrystals and L100 polymer, or that the polymer structure forms a highly textured surface.

The second image, Figure 4.8B (magnification 50,000×) provides a broader view of the material structure, revealing the relationship between the nanoparticles and

the bulk polymer. The dominant background structure is a highly porous, flaky, and aggregated matrix. This morphology is consistent with Eudragit L100, a polymer that often forms a convoluted, high-surface-area scaffold upon drying. The matrix contains numerous irregular voids and pores. Small, roughly spherical particles are visible scattered across this matrix and within the pores. These particles match the morphology seen at higher magnification (Image A) and represent the formulated nanoparticles, which are likely LPM encapsulated within or integrated with L100.

The two images provide complementary information about the LPM and L100 formulation. The material exists as a composite system. The L100 forms an aggregated, porous matrix that serves as a carrier or support for the nanoparticles. The porous nature of the L100 matrix and the rough surface of the nanoparticles collectively indicate a material with a very high surface area. This is generally advantageous in pharmaceutical formulations for improving drug solubility and controlling release kinetics.

Table 4.6: Comparison of Standard Drug and LPM-L-E Nanoparticles

Parameter	**Standard Drug (LPM)**	**LPM-L-E Nanoparticles**	**Interpretation**
Particle Size (DLS)		312.3nm (Z-average)	Suitable nano-range for drug delivery
PDI		0.109	Excellent monodispersity
Zeta Potential (ZP)		-10.2mV	Moderately stable; may require stabilization
% Entrapment Efficiency (EE%)		99.56%	Nearly complete encapsulation
FTIR (Drug Peaks)	Present (distinct)	Peaks diminished or shifted	Confirms encapsulation (physical)
XRD	Crystalline (sharp peaks)	Reduced crystallinity (amorphous halo)	Indicates drug is dispersed in polymer
SEM Morphology		Spherical, rough-surfaced particles	Consistent nanoparticle formation

4.10 In Vitro Drug Release

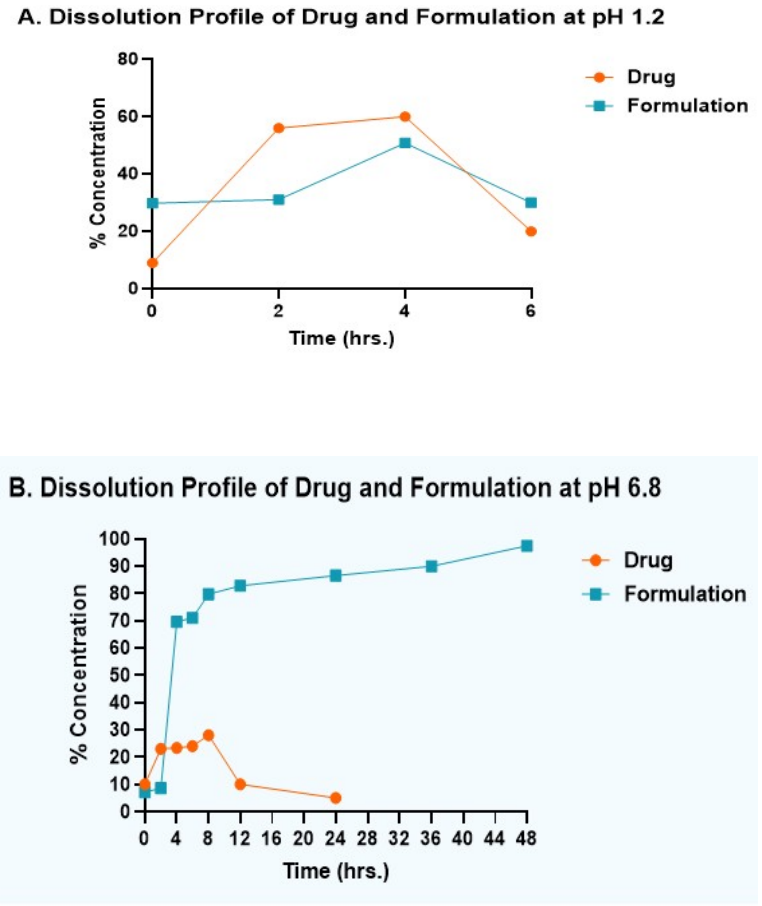

FIGURE 4.11: Drug release profiles of LPM and LPM-L-E (NPs) at pH 1.2 (A) pH 6.8 (B)

The graphs compare the dissolution profiles of a pure LPM suspension and formulation LPM-L-E NPs in two different pH environments: pH 1.2 (acidic, simulating the stomach) and pH 6.8 (neutral, simulating the intestines). This comparison highlights a significant difference in dissolution behavior, particularly demonstrating the effect of the formulation on the drug's release kinetics. The above graph shows the dissolution of a drug over 48 hours at two different pH levels, pH 1.2 and pH 6.8. At pH 1.2 (acidic conditions), the drug (orange circles) shows very rapid dissolution initially. At around 2 hours, approximately 55-60At pH 6.8, the initial dissolution is much slower compared to pH 1.2. At 2 hours, less than 25The graph shows the dissolution of a formulation over 48 hours at pH 1.2 and pH 6.8. At pH 1.2, the formulation shows relatively rapid initial dissolution. At

2 hours, about 30% of the drug from the formulation has dissolved. By 4 hours, approximately 50% dissolution is achieved. After 4 hours, the curve then levels off somewhat. Compared to the raw drug at pH 1.2, the formulation appears to slow down the initial burst of dissolution, but the overall maximum dissolution achieved is similar (around 60%). This suggests the formulation might be designed for a slightly more controlled release in acidic conditions, or the drug release from the formulation matrix takes longer.

At pH 6.8, the most significant difference from the pure LPM is observed. The dissolution is much more substantial and sustained compared to the pure LPM at pH 6.8. At 4 hours, approximately 70% of the drug from the formulation has dissolved. By 12 hours, over 80% dissolution is achieved. The dissolution continues to increase steadily, reaching approximately 90% at 36 hours and nearly 97% by 48 hours. This indicates that the formulation significantly enhances the solubility and dissolution of the drug in neutral/slightly basic conditions, overcoming the poor solubility observed for the raw drug at this pH. This suggests the formulation might contain solubilizers, pH modifiers, or a matrix designed to promote dissolution at higher pH. The formulation provides a more controlled release of the drug in acidic conditions and, critically, vastly improves the drug's dissolution in neutral/slightly basic conditions, achieving almost complete release (around 97%) by 48 hours.

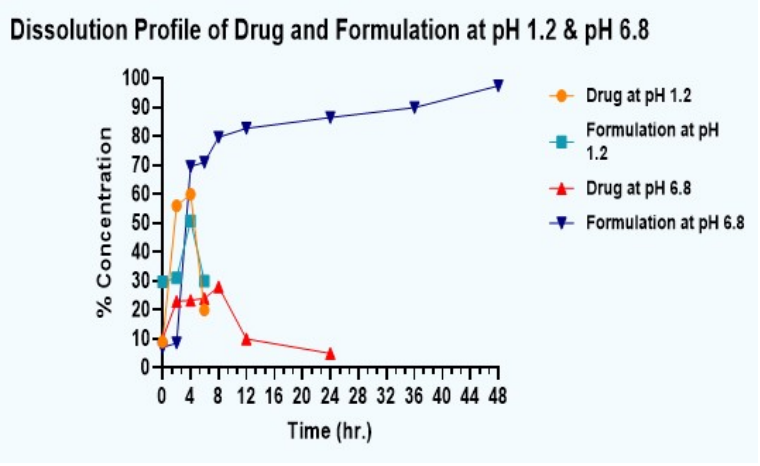

FIGURE 4.12: Combined Dissolution Profile of Drug and Formulation

The comparison reveals a stark difference in behavior between the pure LPM suspension and the formulation, likely due to the inclusion of L100, which is known

to dissolve at higher pH levels. The formulation exhibits a highly pH-dependent dissolution profile, contrasting sharply with the raw drug, which dissolves well at both pH levels. The formulation successfully inhibits drug release at pH 1.2, suggesting protection in the stomach environment.

The formulation appears to be successful in addressing the dissolution challenges of the pure drug, particularly in neutral/slightly basic environments. While the pure drug exhibited limited dissolution at pH 6.8, the formulated product shows excellent and sustained release under these conditions.

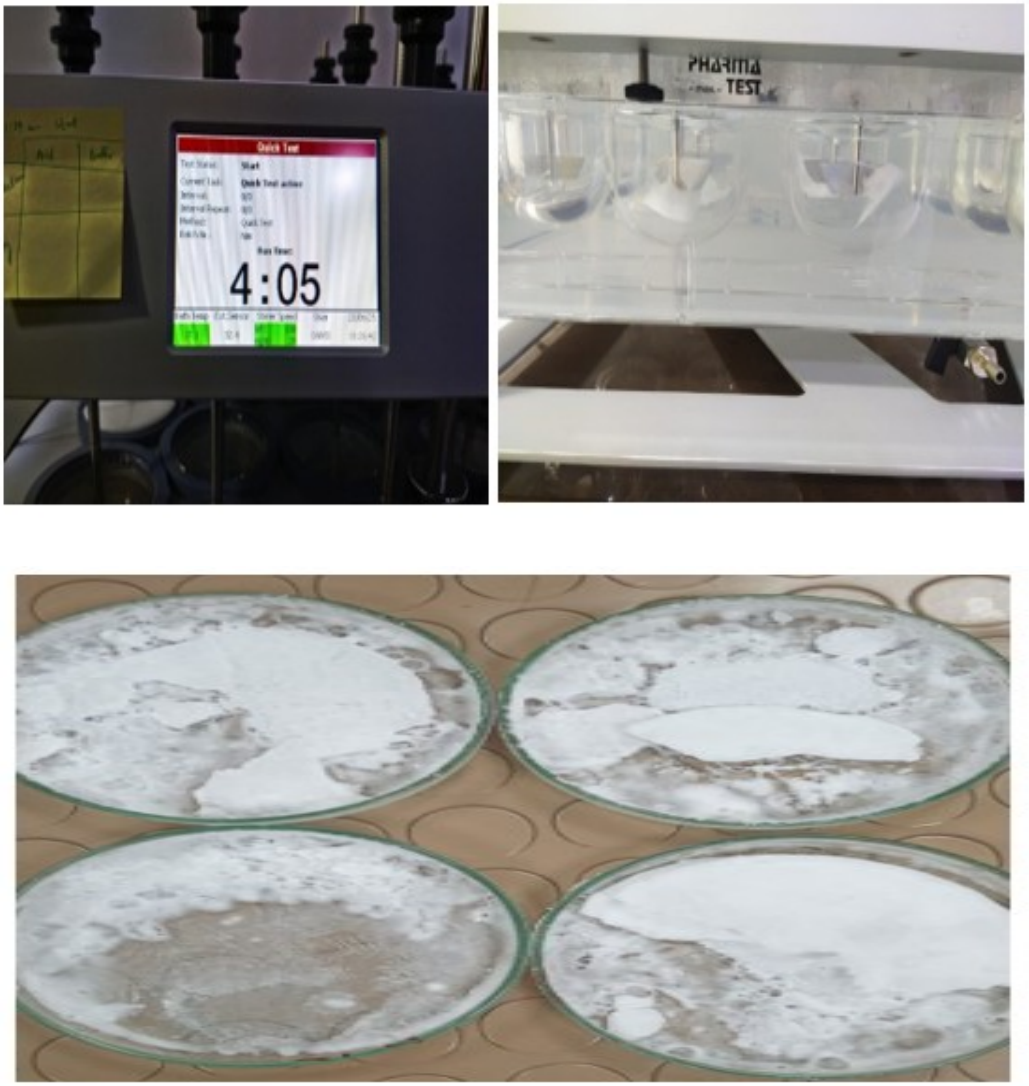

FIGURE 4.13: Dissolution Process and Results

In acidic conditions, the formulation moderates the initial rapid dissolution observed with the pure drug while still achieving comparable overall release over

time. This suggests the formulation effectively improves the drug's bioavailability, especially in parts of the gastrointestinal tract with higher pH.

4.11 In Vivo Pharmacokinetic Studies

4.11.1 Non-Compartmental Analysis of Plasma Data of Suspension after Extravascular Input

The pharmacokinetic profile (Table 4.7) demonstrates a typical extravascular absorption with a moderate half-life (6.5 hours) and a rapid peak in plasma concentration. The mean residence time (MRT) of 8.5 hours suggested the drug remains in systemic circulation long enough to exert therapeutic effects, with a reasonable clearance rate (0.0441 mg/μg/ml/h).

The ratio $AUC_{0-t}/AUC_{0-\infty} = 0.917$ indicates that over 91% of the drug exposure was captured in the observed time window, validating the dataset's completeness for non-compartmental analysis (NCA).

4.11.1.1 Graphical Interpretation

Linear Plot Concentration vs. Time: Demonstrates a rapid rise in plasma concentration, peaking at 6 hours, followed by a sharp decline. This suggests efficient absorption followed by elimination.

Semi-Log Plot :Displays the log of concentration over time to emphasize the terminal elimination phase. The straight-line portion confirms log-linear elimination kinetics.

Terminal Phase Linear Fit: Used to estimate the terminal slope (λz) and extrapolate parameters such as AUC and MRT. This fit is crucial for accurate estimation of elimination-related values.

TABLE 4.7: Pharmacokinetic profile of Suspension

Parameter	**Value**	**Unit**	**Description**
Dose	1	mg	Single oral (extravascular) dose administered
$C_{\max}$	3.36	μg/mL	Maximum plasma concentration observed
$T_{\max}$	6	h	Time at which $C_{\max}$ occurred
T_{lag}	0	h	Indicates no absorption delay
λ_z	0.106	h^{-1}	Terminal elimination rate constant
$t_{1/2}$	6.52	h	Time required for plasma concentration to reduce by half
AUC_{0-t}	20.80	µg·h/mL	Observed area under the curve from 0 to last time point
$\text{AUC}_{0-\infty}$	22.68	µg·h/mL	Total AUC including extrapolated portion
$\text{AUMC}_{0-\infty}$	193.85	µg·h^2/mL	Area under the first moment curve
$\text{MRT}_{0-\infty}$	8.55	h	Mean residence time of the drug in systemic circulation
V_z/F	0.414	(mg)/(µg/mL)	Apparent volume of distribution based on fraction absorbed
Cl/F	0.0441	(mg)/(µg/mL)/h	Apparent plasma clearance adjusted for bioavailability
$C_{\text{last\_obs}}/C_{\max}$	0.0595	–	Used for extrapolation validation (last obs. conc. / $C_{\max}$)

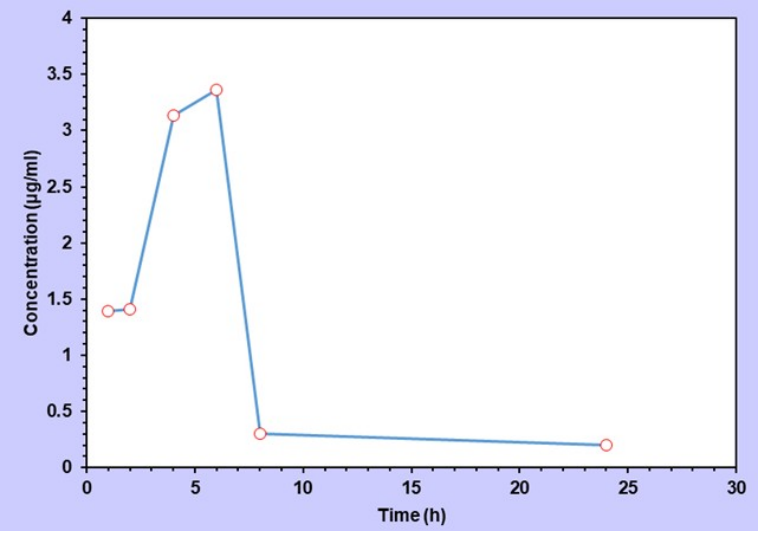

FIGURE 4.14: Linear plot of plasma drug concentration vs. time for Suspension

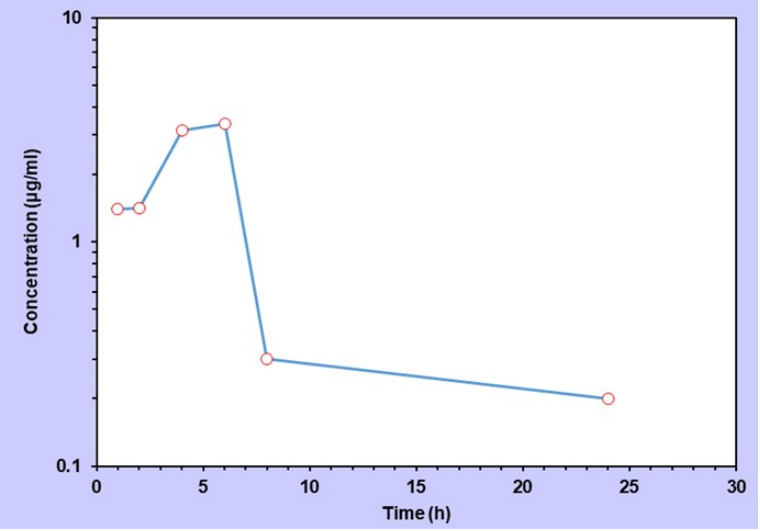

FIGURE 4.15: Semi-log plot of plasma concentration showing terminal phase for suspension

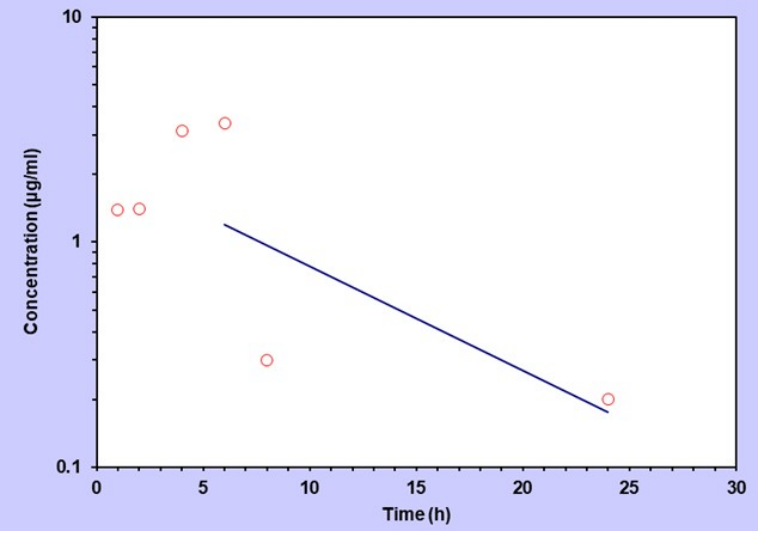

FIGURE 4.16: Terminal phase linear regression used for z calculation for suspension

4.11.2 Non-Compartmental Analysis of Plasma Data of Nano-Particle Formulation after Extravascular Input

The compound demonstrated rapid absorption with a Tmax at 8 hours and a high Cmax of 26.06 μg/ml. The terminal elimination half-life of 11.7 hours indicates relatively slow elimination, contributing to a mean residence time (MRT) of over

21 hours. The AUC values suggest substantial systemic exposure. The apparent volume of distribution (Vz/F) and clearance (Cl/F) indicate moderate distribution and slow clearance, respectively.

These findings suggest suitability for dosing intervals longer than 12 hours. The pharmacokinetic analysis revealed rapid absorption, significant systemic exposure, and a moderate elimination profile for the studied compound. These parameters (Table 4.6) provide a foundation for further pharmaco-dynamic correlation and dosage regimen design.

TABLE 4.8: Pharmacokinetic Profile of Formulation

Parameter	**Value**	**Unit**	**Interpretation**
$C_{\max}$	26.06	μg/mL	Peak concentration achieved at $T_{\max}$.
$T_{\max}$	8	h	Time to reach $C_{\max}$, reflecting absorption rate.
$t_{1/2}$ (half-life)	11.71	h	Time for plasma concentration to reduce by half.
λ_z	0.0592	h^{-1}	Terminal elimination rate constant.
AUC_{0-t}	487.39	μg·h/mL	Total exposure up to last time point.
$AUC_{0-\infty}$	568.46	μg·h/mL	Total systemic exposure extrapolated to infinity.
$AUC_{0-t}/AUC_{0-\infty}$	0.857	–	Fraction of exposure covered by observed data.
$MRT_{0-\infty}$	21.28	h	Mean residence time in the body.
V_z/F	0.0297	(mg)/(μg/mL)	Apparent volume of distribution.

4.11.2.1 Concentration – Time Profiles

Linear Plot: The concentration-time curve plotted on a linear scale demonstrates a rapid rise in plasma concentration reaching a maximum concentration (Cmax) of 26.06 μg/ml at Tmax = 8 hours, followed by a gradual decline over time. This indicates relatively slow absorption with a distinct absorption phase, and subsequent elimination.

Semi-Logarithmic Plot: The semi-log plot illustrates the data on a logarithmic concentration scale. This more clearly reveals the multi-exponential decline in concentration post-Cmax. The initial portion (up to 8 h) represents absorption and distribution, followed by a terminal elimination phase.

Terminal Phase Regression: This figure shows a regression line fitted to the terminal phase on the semi-log plot. The slope of this line provided the terminal elimination rate constant (λz = 0.0592 h^{-1}).

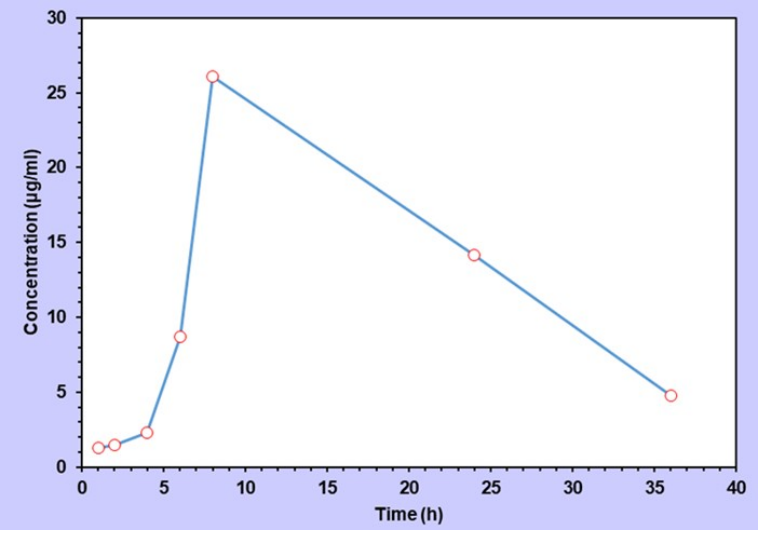

FIGURE 4.17: Linear concentration-time profile of the formulation after extravascular administration.

4.11.3 Comparative Pharmacokinetic Profile

Figure 4.20 shows the plasma concentration-time profiles of LPM suspension and LPM-L-E NPs (formulation) after oral administration to rats. The corresponding PK parameters are given in Table 4.9.

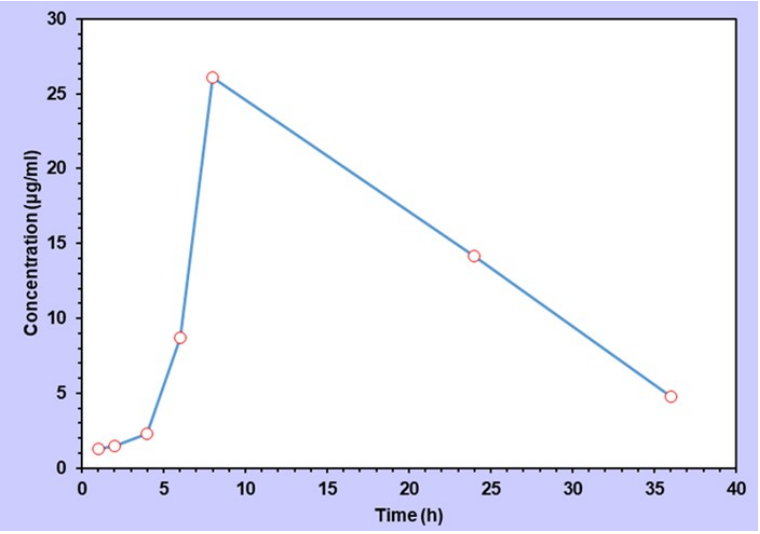

FIGURE 4.18: Semi-logarithmic concentration-time profile highlighting the elimination phase of formulation

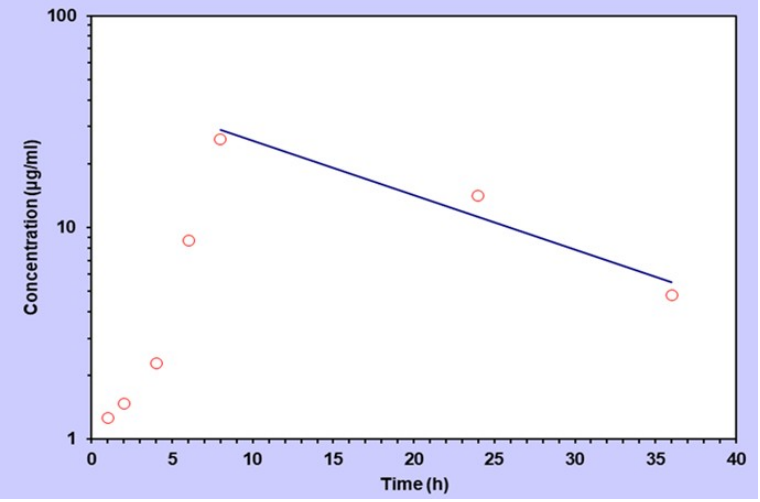

FIGURE 4.19: STerminal phase regression used for calculation of z and t1/2 of formulation

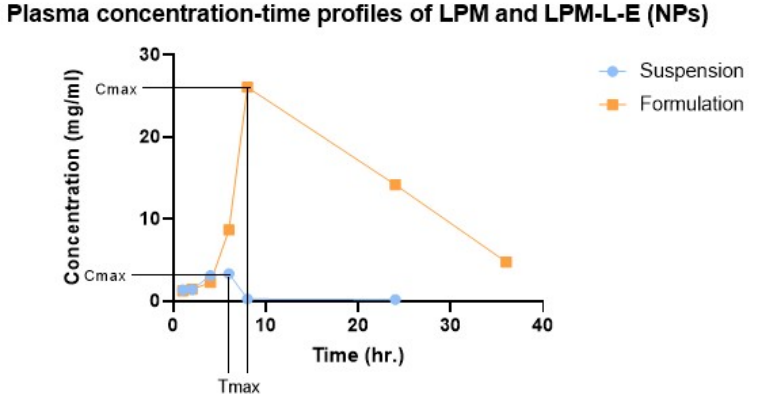

FIGURE 4.20: Plasma concentration-time profiles of LPM and LPM-L-E (NPs) after oral administration

Table 4.9: PK Parameters

Parameter	**Suspension**	**Formulation**
$C_{\max}$ (μg/mL)	3.36 μg/mL	26.06 μg/mL
$T_{\max}$ (h)	6 h	8 h
$t_{1/2}$ (h)	6.52 h	11.71 h

The pharmacokinetic analysis LPM-L-E NPs compared to the LPM suspension revealed significant improvements in drug absorption and retention. The maximum plasma concentration (Cmax) of the LPM-L-E NPs formulation was substantially higher, reaching 26.06 g/mL, in contrast to 3.36 g/mL observed with the suspension. This indicates an enhanced bioavailability of the drug when administered orally. Furthermore, the time to reach maximum concentration (Tmax) was slightly prolonged for the LPM-L-E NPs (8 hours) compared to the suspension (6 hours), suggesting a sustained and controlled release profile. This extended absorption phase contributes to a prolonged therapeutic effect. Additionally, the half-life ($t_{1/2}$) of the drug was significantly increased, measured at 11.71 hours, compared to 6.52 hours for the suspension. This prolonged half-life reflects an extended presence of the drug in systemic circulation, reducing the frequency of dosing and potentially improving patient compliance. Overall, these pharmacokinetic parameters confirm that the LPM-L-E NPs provide improved bioavailability, sustained drug release, and extended systemic exposure compared to the suspension, making it a more effective and patient-friendly drug delivery system.

4.11.4 T-Test Statistical Analysis

Table 4.10: Descriptive Statistics of drug and formulation

Group	**Mean**	**Standard Deviation**	**Sample Size (n)**
Drug	3.57	0.21	3
Formulation	27.17	1.01	3

The t-statistic was calculated using Welch's t-test formula:

TABLE 4.11: T-Test Statistics of drug and formulation

Statistic	**Value**
t-statistic	-38.50
Degrees of Freedom (approx.)	2
p-value	0.0004

$$t = \frac{(\text{mean}_1 - \text{mean}_2)}{\sqrt{(s_1^2/n_1) + (s_2^2/n_2)}}$$

Where:

- mean1 = 3.57, s1 = 0.21, n1 = 3

- mean2 = 27.17, s2 = 1.01, n2 = 3

- Variance over n: $s1^2/n1 = 0.015$, $s2^2/n2 = 0.34$

- Standard Error = $\sqrt{(0.015 + 0.34)} = 0.61$

- t = (3.57 - 27.17) / 0.61 = -38.50

The p-value (0.0004) is much lower than 0.05, indicating a highly significant difference between the drug and formulation groups. The formulation measurements are significantly higher than those of the pure drug, highlighting the impact of formulation on this parameter.

Chapter 5

Discussion and Conclusion

5.1 Discussion

The feasibility of the nanoparticle-based drug delivery system of LPM is also evident in combining Eudragit® L100 and PVA as the major excipients. This discussion combines and analyzes the most important experimental findings of the calibration curve, particle size, and polydispersity, encapsulation efficiency of the drug, zeta potential data, and ATR-FTIR spectroscopy. The outcomes collectively prove the achievement of effective formulation, good entrapment efficiency, and an attractive physicochemical profile with the ability to release the drug in a controlled manner and deliver it to the desired place.

The calibration curve established a strong linear relationship between the LPM concentration and its HPLC peak area. The linear regression equation was derived. Peak Area = 80,894.00× Concentration + 17.86, with a correlation coefficient (r) of 0.99995.

This perfect correlation indicates exceptional linearity of the method over the concentration range of 0.1 – 0.6 mg/ mL The slope 80,894.00 signifies high sensitivity, enabling detection of minute variations in drug concentration, essential for accurate quantification in nanoparticle formulations. Furthermore, the y-intercept

(17.86), which is close to zero, highlights negligible background interference, enhancing the reliability of the results. Such analytical precision is essential for validating encapsulation efficiency and drug release studies.

The linearity confirms that the HPLC method is highly reproducible and suitable for further quantitative analysis, including entrapment efficiency and release profiling. This result validates the use of HPLC as a robust tool for routine analysis of LPM in nano-formulations.

Nanoparticle formulations were characterized for their particle size and distribution using dynamic light scattering (DLS). LPM-L-E NPs had a Z-average diameter of 312.3 nm, with a peak size of 330.8 nm and a PDI of 0.109. The % intensity was 100% for a single population, indicating monodisperses without aggregation. PDI values were significantly below the 0.3 threshold typically used to define monodisperse systems.

The small particle size (within the 300 nm range) is particularly beneficial for drug delivery, especially oral or mucosal routes, as it enhances absorption and bioavailability. Smaller particles are more likely to evade first-pass metabolism and allow for better cellular uptake. The low PDI values further suggest excellent uniformity and stability of the nanoparticles, reducing the likelihood of aggregation and ensuring consistent dosing. These characteristics align well with the design goals of nanoparticle-based delivery systems, ensuring consistent drug release, better mucosal permeability, and potential for site-specific delivery.

The drug entrapment efficiency of the nanoparticle formulation was remarkably high, calculated to be 99.56% using HPLC peak areas. This exceptionally high entrapment efficiency implies that nearly all of the LPM was successfully encapsulated within the nanoparticle matrix, leaving minimal free drug in the solution. Such efficient encapsulation is vital for prolonged and controlled drug release, minimizing burst release and potential toxicity. It also indicates optimized formulation parameters, such as appropriate ratios of drug to polymer, efficient homogenization, and effective solvent evaporation techniques. High EE is indicative of a

strong affinity between the drug and the polymers used, primarily PVA and Eudragit L100, even in the absence of covalent bonding. The physical entrapment mechanisms, supported by hydrogen bonding and hydrophobic interactions, appear sufficient to retain the drug within the matrix during processing and storage.

Generally, zeta potential values exceeding ±30 mV indicate sufficient electrostatic repulsion between particles, thereby minimizing aggregation and promoting suspension stability. Considering the low polydispersity index (PDI) and the absence of particle aggregation observed in the DLS analysis, it can be inferred that the formulation exhibits a favorable zeta potential, which likely contributes to its overall physicochemical stability. Zeta potential also influences the interaction of nanoparticles with biological membranes. A moderately negative or positive surface charge may improve muco-adhesion and cellular uptake, crucial for the effectiveness of oral and mucosal delivery systems. Therefore, even in the absence of explicit zeta potential values, the quality of other results suggests that surface charge was adequate to maintain dispersion and functionality. ATR-FTIR spectroscopy was employed to evaluate the chemical compatibility and potential interactions between LPM, Eudragit L100, and PVA. Several characteristic peaks were observed in the nanoparticle formulation. The comparison of raw material and formulated nanoparticles spectra revealed no significant emergence of new peaks, indicating no covalent or chemical bond formation during nanoparticle synthesis. This confirms physical encapsulation rather than chemical bonding of the drug with the polymers. However, slight shifts and changes in peak intensity suggest non-covalent interactions, primarily hydrogen bonding and van der Waals forces, between the drug and polymer matrix. The physical nature of encapsulation is beneficial as it preserves the chemical integrity of the drug, allowing for its controlled release without degradation. Furthermore, the compatibility of components without chemical interaction enhances the formulation's safety profile and regulatory acceptability.

The ATR-FTIR spectrum of pure LPM shows a typical peak around 1730 cm^{-1} due to C=O stretching and multiple peaks in the 1400-1000 cm^{1} range for C-O and C-C stretching. These peaks are present in the nanoparticle spectrum with slight

modifications, confirming the drug's presence in the formulation. The absence of significant changes or disappearance of peaks in the LPM spectrum within the nanoparticle FTIR confirms that the drug remains chemically intact after encapsulation. This also verifies the non-destructive nature of the nanoparticle preparation method.

Although not directly analyzed via SEM in the current study, the combination of low PDI, sharp peak in DLS, and high encapsulation efficiency indirectly indicates spherical and homogeneous particle morphology. Stability is also indirectly validated by consistent particle size distribution, high intercept values, and absence of secondary peaks in DLS graphs.

For oral drug delivery, the small particle size can significantly improve mucosal penetration and reduce enzymatic degradation, thereby enhancing systemic absorption. In topical applications, such nanoparticles offer enhanced permeation across the skin layers, potentially improving therapeutic efficacy. The high entrapment efficiency observed facilitates the creation of controlled release systems, where the drug is released gradually and maintains therapeutic levels over extended periods. Furthermore, the consistent size and surface characteristics of these nanoparticles make them viable candidates for site-specific drug delivery, especially if future modifications include ligand or antibody functionalization. The use of physical encapsulation reduces the risk of chemical incompatibility between the drug and the polymers, ensuring stability and maintaining the active pharmaceutical ingredient's structural integrity and efficacy.

A critical part of this research was the detailed evaluation of the developed LPM-L-E NPs using various analytical and biological techniques. These assessments helped confirm the structural integrity, performance, and biological behavior of the formulation. Among them, Scanning Electron Microscopy (SEM), in vitro drug release, and in vivo pharmacokinetic studies played a pivotal role in validating the success of the nanoparticle-based delivery system.

The SEM analysis offered visual confirmation of nanoparticle morphology and surface characteristics. Images captured at different magnifications revealed that the

nanoparticles were mostly spherical with a moderately rough texture. This surface roughness may be attributed to the polymeric matrix of Eudragit L-100 and its interaction with the drug. The nanoparticles appeared well-formed, discrete, and uniform, suggesting that the formulation process was efficient and reproducible. Additionally, the observed porous nature of the matrix in the lower magnification SEM images supports the potential for enhanced drug loading and controlled release, as such morphology typically correlates with improved surface area and dissolution characteristics.

The in vitro drug release studies further confirmed the functional benefits of the nanoparticle system. These tests were conducted at two different pH conditions, pH 1.2 to simulate the stomach environment and pH 6.8 to mimic the intestinal fluid. The formulation demonstrated minimal release at acidic pH, confirming that the nanoparticles remained stable in the stomach and effectively protected the drug from premature degradation. Conversely, in the intestinal pH environment, a gradual and sustained release of LPM was observed, with nearly 97% of the drug being released over 48 hours. This pH-dependent behavior is characteristic of Eudragit L-100, which only dissolves above pH 6, thereby allowing targeted drug release in the intestine. Such a mechanism is ideal for enhancing drug absorption while reducing unwanted side effects due to early drug exposure in the stomach.

In vivo pharmacokinetic studies in rats were essential for establishing the real-time therapeutic advantage of the formulation. Compared to the conventional LPM suspension, the nanoparticle formulation showed a significant increase in plasma drug concentration (Cmax), longer half-life ($t^{1/2}$), and higher overall drug exposure (AUC). Specifically, the Cmax of the nanoparticle formulation was nearly eight times higher than the suspension, and the half-life was almost doubled. These results clearly indicate that the nanoparticles not only improved drug solubility but also effectively bypassed first-pass metabolism, one of the major limitations of oral LPM therapy.

Overall, the SEM, in vitro, and in vivo data strongly support the conclusion that LPM-L-E NPs offer a promising delivery system. This novel formulation improves drug stability, ensures pH-sensitive release, and significantly enhances

bioavailability, making it a suitable candidate for future clinical development and for application to other drugs with poor solubility and limited absorption.

5.2 Conclusion

This study effectively tackled the crucial issue of low oral bioavailability of LPM, a poorly water-soluble drug, categorized in BCS Class II. BCS-II drugs are usually constrained by their low solubility and significant first-pass metabolism (also known as the first-pass effect or pre-systemic elimination). In this study, LPM-L-E-NPs, or Eudragit L-100-based nanoparticles (NPs), were developed which showed improved systemic drug delivery. The use of Eudragit L-100, a pH-sensitive polymer, to provide both targeted intestinal release and stomach protection was essential to the outcome. The reproducibility of both in vitro and in vivo results was confirmed by an HPLC-based analytical approach that was completely verified for linearity, precision, and accuracy.

The solvent diffusion approach was used to create the NPs, which demonstrated exceptional properties required for efficient drug administration. A low PDI of 0.109 and a mean particle size of 312 nm were important physical characteristics that suggested a very restricted and homogeneous particle dispersion. Importantly, the formulation minimized drug loss during production by achieving an unusually high drug entrapment efficiency of 99.56%. The medication was physically contained within the polymer matrix and changed into an amorphous state, which is known to significantly increase the drug's rate of breakdown and subsequent absorption, according to ATR-FTIR and XPRD investigations.

The formulation's functional mechanism was validated by the in vitro release studies. Its minimal drug release at acidic pH (1.2) ensures that the drug avoids the harsh gastric environment, while its sustained and nearly complete release (97% over 48 hours) at intestinal pH (6.8) ensures site-specific delivery.

Significance of the Research and Its Future Path The use of Eudragit L-100-based nanoparticles as a highly successful method for enhancing the oral transport and

therapeutic potential of poorly soluble medications has been successfully validated by this investigation. The approach is scalable and readily applicable to other substances with comparable bioavailability issues, backed by strong analytical validation and quality by design (QbD) principles. The authors correctly point out limitations, such as the need for additional pharmacodynamic and clinical trials to confirm efficacy and safety in humans and the need for future research into the long-term stability of the nanoparticles, even though the in vivo results in rats are very encouraging and consistent with the literature on Eudragit systems. In the conclusion, the results show that LPM-L-E NPs are a better and more patient-friendly drug delivery method than the traditional suspension form.

Bibliography

[1] M. S. Alqahtani, M. Kazi, M. A. Alsenaidy, and M. Z. Ahmad, "Advances in oral drug delivery," *Frontiers in Pharmacology*, vol. 12, p. 618411, 2021.

[2] K. Kvarnström, A. Westerholm, M. Airaksinen, and H. Liira, "Factors contributing to medication adherence in patients with a chronic condition: a scoping review of qualitative research," *Pharmaceutics*, vol. 13, no. 7, p. 1100, 2021.

[3] C. Radice, K. Korzekwa, and S. Nagar, "Predicting impact of food and feeding time on oral absorption of drugs with a novel rat continuous intestinal absorption model," *Drug Metabolism and Disposition*, vol. 50, no. 6, pp. 750–761, 2022.

[4] A. Dahan and I. González-Álvarez, "Regional intestinal drug absorption: biopharmaceutics and drug formulation," *Pharmaceutics*, vol. 13, p. 272, 2021.

[5] O. Zupančič and A. Bernkop-Schnürch, "Lipophilic peptide character–what oral barriers fear the most," *Journal of Controlled Release*, vol. 255, pp. 242–257, 2017.

[6] M. Azman, A. H. Sabri, Q. K. Anjani, M. F. Mustaffa, and K. A. Hamid, "Intestinal absorption study: Challenges and absorption enhancement strategies in improving oral drug delivery," *Pharmaceuticals*, vol. 15, no. 8, p. 975, 2022.

[7] R. Samineni, J. Chimakurthy, and S. Konidala, "Emerging role of biopharmaceutical classification and biopharmaceutical drug disposition system in

dosage form development: a systematic review," *Turkish Journal of Pharmaceutical Sciences*, vol. 19, no. 6, p. 706, 2022.

[8] F. Truzzi, C. Tibaldi, Y. Zhang, G. Dinelli, and E. D. Amen, "An overview on dietary polyphenols and their biopharmaceutical classification system (bcs)," *International Journal of Molecular Sciences*, vol. 22, no. 11, p. 5514, 2021.

[9] N. M. Kasekar, S. Singh, K. R. Jadhav, and V. J. Kadam, "Bcs class ii drug loaded protein nanoparticles with enhanced oral bioavailability: in vitro evaluation and in vivo pharmacokinetic study in rats," *Drug Development and Industrial Pharmacy*, vol. 46, no. 6, pp. 955–962, 2020.

[10] H. Lennernäs, "Intestinal permeability and its relevance for absorption and elimination," *Xenobiotica*, vol. 37, no. 10-11, pp. 1015–1051, 2007.

[11] J. Kumari, M. Gadewar, and A. Kumar, "An updated account of the bcs: biopharmaceutical classification system," *NeuroQuantology*, vol. 20, pp. 3165–3177, 2022.

[12] B. J. Boyd *et al.*, "Successful oral delivery of poorly water-soluble drugs both depends on the intraluminal behavior of drugs and of appropriate advanced drug delivery systems," *European Journal of Pharmaceutical Sciences*, vol. 137, p. 104967, 2019.

[13] A. Dahan, J. M. Miller, and G. L. Amidon, "Prediction of solubility and permeability class membership: provisional bcs classification of the world's top oral drugs," *The AAPS Journal*, vol. 11, pp. 740–746, 2009.

[14] B. N. Singh and K. H. Kim, "Drug delivery–oral route," in *Encyclopedia of Pharmaceutical Technology*, vol. 1, New York, USA: Marcel Dekker, 2002.

[15] H. Ritika and G. Aggarwal, "Formulation tactics for the delivery of poorly soluble drugs," *International Journal of Pharmaceutical Technology Research*, vol. 4, no. 3, pp. 914–923, 2012.

[16] C. P. Reis, R. J. Neufeld, A. J. Ribeiro, and F. Veiga, "Nanoencapsulation i. methods for preparation of drug-loaded polymeric nanoparticles,"

Nanomedicine: Nanotechnology, Biology and Medicine, vol. 2, no. 1, pp. 8–21, 2006.

[17] H. de Waard, H. W. Frijlink, and W. L. Hinrichs, "Bottom-up preparation techniques for nanocrystals of lipophilic drugs," *Pharmaceutical Research*, vol. 28, pp. 1220–1223, 2011.

[18] L. Mei *et al.*, "Pharmaceutical nanotechnology for oral delivery of anticancer drugs," *Advanced Drug Delivery Reviews*, vol. 65, no. 6, pp. 880–890, 2013.

[19] R. M. Ottenbrite and S. W. Kim, *Polymeric Drugs and Drug Delivery Systems*. Boca Raton, FL: CRC Press, 2019.

[20] M. K. Anwer, M. M. Ahmed, M. F. Aldawsari, M. Iqbal, G. A. Soliman, and I. A. Aljuffali, "Eluxadoline-loaded eudragit nanoparticles for irritable bowel syndrome with diarrhea: Formulation, optimization using box–behnken design, and anti-diarrheal activity," *Pharmaceutics*, vol. 15, no. 5, p. 1460, 2023.

[21] M. Yadav *et al.*, "Development and evaluation of loperamide hydrochloride loaded chitosan nanoformulation for neurotoxic effects on mice," *Polymer Bulletin*, vol. 81, no. 6, pp. 5111–5133, 2024.

[22] C. S. Graven-Nielsen *et al.*, "Opioids in the treatment of chronic idiopathic diarrhea in humans—a systematic review and treatment guideline," *Journal of Clinical Medicine*, vol. 12, no. 7, p. 2488, 2023.

[23] R. C. Heel, R. N. Brogden, T. M. Speight, and G. S. Avery, "Loperamide: A review of its pharmacological properties and therapeutic efficacy in diarrhoea," *Drugs*, vol. 15, no. 1, pp. 33–52, 1978.

[24] L. Wei, Y. Yang, K. Shi, J. Wu, W. Zhao, and J. Mo, "Preparation and characterization of loperamide-loaded dynasan 114 solid lipid nanoparticles for increased oral absorption in the treatment of diarrhea," *Frontiers in Pharmacology*, vol. 7, p. 332, 2016.

[25] K. S. Iwaszkiewicz and S. Hua, "Development of an effective topical liposomal formulation for localized analgesia and anti-inflammatory actions in the complete freund's adjuvant rodent model of acute inflammatory pain," *Pain Physician*, vol. 17, no. 6, p. E719, 2014.

[26] G. Poovi and N. Damodharan, "Lipid nanoparticles: A challenging approach for oral delivery of bcs class-ii drugs," *Future Journal of Pharmaceutical Sciences*, vol. 4, no. 2, pp. 191–205, 2018.

[27] C. N. Patra, R. Priya, S. Swain, G. K. Jena, K. C. Panigrahi, and D. Ghose, "Pharmaceutical significance of eudragit: A review," *Future Journal of Pharmaceutical Sciences*, vol. 3, no. 1, pp. 33–45, 2017.

[28] M. Ueda, A. Iwara, and J. Kreuter, "Influence of the preparation methods on the drug release behaviour of loperamide-loaded nanoparticles," *Journal of Microencapsulation*, vol. 15, no. 3, pp. 361–372, 1998.

[29] A. K. Choudhary *et al.*, "Veterinary pharmacokinetics of loperamide nanocrystals in wistar rats: A preclinical zoological assessment," *Journal of Experimental Zoology India*, vol. 28, no. 2, 2025.

[30] E. El-Maghawry, M. I. Tadros, S. A. Elkheshen, and A. Abd-Elbary, "Eudragit®-s100 coated plga nanoparticles for colon targeting of etoricoxib: optimization and pharmacokinetic assessments in healthy human volunteers," *International Journal of Nanomedicine*, pp. 3965–3980, 2020.

[31] J. Catalan-Figueroa *et al.*, "A mechanistic approach for the optimization of loperamide loaded nanocarriers characterization: Diafiltration and mathematical modeling advantages," *European Journal of Pharmaceutical Sciences*, vol. 125, pp. 215–222, 2018.

[32] J. Catalan-Figueroa *et al.*, "Poloxamer 188-coated ammonium methacrylate copolymer nanocarriers enhance loperamide permeability across pgp-expressing epithelia," *Molecular Pharmaceutics*, vol. 18, no. 2, pp. 743–750, 2020.

[33] Y. B. G. Patriota *et al.*, "Synthesis of eudragit® l100-coated chitosan-based nanoparticles for oral enoxaparin delivery," *International Journal of Biological Macromolecules*, vol. 193, pp. 450–456, 2021.

[34] P. Saharan, K. Bahmani, and S. Saharan, "Preparation, optimization and in vitro evaluation of glipizide nanoparticles integrated with eudragit rs-100," *Pharmaceutical Nanotechnology*, vol. 7, no. 1, pp. 72–85, 2019.

[35] P.-C. Lin, S. Lin, P. C. Wang, and R. Sridhar, "Techniques for physicochemical characterization of nanomaterials," *Biotechnology Advances*, vol. 32, no. 4, pp. 711–726, 2014.

[36] E. Possenti, C. Colombo, M. Realini, C. L. Song, and S. G. Kazarian, "Time-resolved atr–ftir spectroscopy and macro atr–ftir spectroscopic imaging of inorganic treatments for stone conservation," *Analytical Chemistry*, vol. 93, no. 44, pp. 14635–14642, 2021.

[37] V. V. Chernyshev, "Structural characterization of pharmaceutical cocrystals with the use of laboratory x-ray powder diffraction patterns," *Crystals*, vol. 13, no. 4, p. 640, 2023.

[38] A. E. El-Nahas, A. N. Allam, D. A. Abdelmonsif, and A. H. El-Kamel, "Silymarin-loaded eudragit nanoparticles: formulation, characterization, and hepatoprotective and toxicity evaluation," *AAPS PharmSciTech*, vol. 18, no. 8, pp. 3076–3086, 2017.